

# Self-consistent Gutzwiller study of *bcc* Fe: interplay of ferromagnetic order and kinetic energy

Giovanni Borghi,<sup>1,2</sup> Michele Fabrizio,<sup>2</sup> and Erio Tosatti<sup>2,3,4</sup>

<sup>1</sup>*Theory and Simulation of Materials, École Polytechnique Fédérale de Lausanne EPFL, CH-1015 Lausanne, Switzerland.*

<sup>2</sup>*International School for advanced studies (SISSA), via Bonomea 265, 34136 Trieste, Italy.*

<sup>3</sup>*CNR-IOM Democritos, via Bonomea 265, 34136 Trieste, Italy.*

<sup>4</sup>*International Centre for Advanced Studies, Strada Costiera 11, 34151 Trieste, Italy.\**

The Gutzwiller technique has long been known as a method to include correlations in electronic structure calculations. Here we implement an *ab-initio* Gutzwiller+LDA calculation exposing the detailed protocol step by step, in a way that should be of use for future applications. We apply it to a classic problem, the ferromagnetism of bulk *bcc* Fe, whose nature has attracted recent interest. In the conventional Stoner-Wohlfarth model, the ferromagnetic ordering of iron sets in so that the electrons can reduce their mutual Coulomb repulsion—naturally at the extra cost of some increase of electron kinetic energy. Density functional theory within the spin polarized local density approximation (LDA) calculations has long supported that picture, showing that ferromagnetic alignment causes band narrowing and a corresponding wavefunction localization, whence a kinetic energy increase. However, because of its inadequate treatment of strong intra-site correlations for localized *d* orbitals, LDA cannot be relied upon, particularly when it comes to separately describing fine potential and kinetic energy imbalances. With *ab-initio* Gutzwiller+LDA, we indeed find that the effect of correlations is to dramatically reverse the balance, the ferromagnetic ordering of Fe in fact causing a decrease of kinetic energy, at the cost of some increase of potential energy. The underlying physical mechanism, foreshadowed long ago by Goodenough and others, and more recently supported by LDA-DMFT calculations, is that correlations cause  $e_g$  and  $t_{2g}$   $3d$  orbitals to behave very differently. Weakly dispersive  $e_g$  states are spin-polarized and almost localized, while, more than half filled, the  $t_{2g}$  are broad band, fully delocalized states. Owing to intra-atomic Hund's rule exchange which aligns  $e_g$  and  $t_{2g}$  spins, the propagation of itinerant  $t_{2g}$  holes is only allowed when different atomic spins are ferromagnetically aligned. We thus conclude that double exchange is at work already in the most popular ferromagnetic metal.

## INTRODUCTION

The conduction electron Wannier orbitals in transition-metal compounds are generally fairly localized in space so that electronic correlations, i.e. all effects that deviate from the independent-particle picture, are sometimes strong enough to give rise to metal-insulator transitions in particular temperature and pressure conditions. The correlation-driven metal-insulator transition, known as Mott transition,<sup>1,2</sup> is often accompanied by rather spectacular phenomena that appear in its proximity, high-temperature superconductivity being the most popular example. This makes  $3d$  metal elements and compounds a natural laboratory for intriguing many-body physics, which despite a rich history and many studies is worth exploring further.

Electronic structure methods (sometimes referred to as "first principles" methods) that rely on independent particle descriptions, such as Hartree-Fock (HF) or Density Functional Theory (DFT) within Local Density Approximation (LDA), are by construction incapable of capturing the Mott transition, which has no counterpart in a one electron picture. For this reason, HF and LDA, while generally quite successful for many materials, may sometimes fail in the description of solids involving transition metals. In fact, most of our knowledge about Mott electron localization has been attained by means of simplified lattice models, the best known being the

Hubbard model,<sup>3</sup> which are accessible by methods better suited to deal with correlations, such as quantum Monte Carlo,<sup>4</sup> density-matrix renormalization group<sup>5</sup> and dynamical mean-field theory.<sup>6</sup>

Clearly, for the purpose of a quantitative understanding of real materials, it is of key importance to sew the two worlds together, bringing in particular the many body expertise gained on lattice models over to realistic, off-lattice, first-principles calculations of solids.

This has historically been attempted through ad-hoc improvements of DFT. For instance, the inclusion (in fact, the addition and subtraction) of an intra-site Coulomb repulsion  $U$  (the "Hubbard  $U$ ") in the Kohn-Sham Hamiltonian permits a decrease of the so-called self-interaction error, a severe flaw of LDA for partially or fully occupied localized orbitals – just the case of transition metals. When added to LDA, this procedure, the so called Local Density Approximation plus Hubbard- $U$  (LDA+ $U$ ),<sup>7,8</sup> often improves results, and can for example stabilize magnetic phases which straight LDA would miss. Yet, LDA+ $U$  remains basically a mean-field, independent particle approach that cannot describe Mott localization. The problem can be overcome if, for instance, the Kohn-Sham Hamiltonian of LDA supplemented by  $U$  is solved through Dynamical Mean-Field Theory (DMFT), by the so-called Local Density Approximation plus Dynamical Mean-Field Theory (LDA+DMFT).<sup>9</sup> Alternatively, variational Quantum

Monte Carlo Variational Quantum Monte Carlo (VQMC) approaches<sup>10,11</sup> have been successfully applied to the electronic properties of atoms and simple molecules,<sup>12</sup> and its development appears to be promising for more ambitious applications.

At present, both LDA+DMFT and VQMC are numerically much more involved and far more demanding than conventional LDA or even LDA+U, which owe much of their success to simplicity. The desirability of approaches joining together the simplicity of LDA and the description of correlations typical of many body methods is therefore still very high. In the context of lattice models, a simple approach to strong correlations was proposed long ago by Martin C. Gutzwiller.<sup>13,14</sup> This method, projecting out of a trial Slater determinant an adjustable proportion of costly configurations and evaluating average values by approximate formulas, is strictly variational in the limit of infinite lattice-coordination<sup>15</sup> – the same limit where DMFT is exact – providing much more accurate results than HF. That success invites the use of the Gutzwiller method even when the lattice space dimension, and thus the site coordination, is finite, as people do with DMFT. Gutzwiller Approximation (GA) electronic structure calculations have the great advantage to couple extreme LDA-level simplicity with qualitatively, often quantitatively, increased accuracy in the description of correlations. For example, GA has been able to describe conducting materials that are insulators “in disguise”,<sup>16</sup> i.e. whose properties depend on correlations that are already present in their Mott insulating phase, and that continue to play an important role even in the nearby metallic phases. A well known example is the RVB scenario for high-temperature superconductors,<sup>17</sup> where Cooper pairing is explained as a byproduct of doping a parent state of resonating valence bonds, which is the remnant of antiferromagnetism when Néel long range order disappears. Another famous result of the GA is the Brinkman-Rice description of the Mott transition in vanadium sesquioxide, originally derived by the GA solution to the Hubbard model.<sup>18</sup>

Because of its simplicity, a great deal of effort has therefore been devoted in recent years to extend GA from simple lattice models to more realistic off-lattice cases.<sup>19–25</sup> Here we implement a density self-consistent algorithm that exploits the Gutzwiller variational wave function together with the conventional LDA for the density functional. The Levy-Lieb constrained-search formulation of DFT provides a solid theoretical framework for the introduction of Gutzwiller variational parameters in the density functional, while a localized atomic basis set (we use in particular the Siesta electronic structure code) makes the definition of the Gutzwiller-projected states straightforward.

We test the power of the Local Density Approximation plus Gutzwiller Method (LDA+G) functional by calculating the electronic structure of nonmagnetic and ferromagnetic *bcc* Fe, motivated by long standing basic questions about the electronic origin of magnetic order,<sup>26</sup> in-

cluding a recent LDA+DMFT study by Anisimov and coworkers<sup>27</sup> suggesting that *bcc* iron might be an orbital-selective Mott insulator. According to that picture, the poorly dispersive  $e_g$ -type electrons of metallic Fe may be fully localized due to interactions, so that conduction phenomena are restricted within the  $t_{2g}$  manifold (besides of course the  $s$  electrons). In that picture<sup>28–30</sup> ferromagnetic alignment would not be due to intersite Coulomb exchange, as is ordinarily assumed, but rather to double-exchange, as in colossal magnetoresistance manganites.<sup>31</sup> The Mott localized  $e_g$  electrons form spin-1 moments that couple ferromagnetically via intra-atomic Hund’s exchange to the electrons in the nearly-full itinerant  $t_{2g}$  bands. In order to preserve coherent  $t_{2g}$  hole motion, the local  $e_g$  moments order ferromagnetically. As in the manganites, ferromagnetism is thus driven by a kinetic energy gain rather than a potential energy one. Even though our LDA+G approach is still mean-field and thus cannot address dynamical phenomena such as orbital selective Mott transitions – especially so in a delicate case where the two sets of orbitals,  $e_g$  and  $t_{2g}$ , hybridize with each other in the Brillouin zone – we find that calculation of the total energy and a detailed analysis of its separate kinetic and potential energy contributions actually supports double-exchange as the driving mechanism of ferromagnetism in iron, rather than the conventional Stoner instability. On the whole, this work may also be of general use as a very detailed example of *ab-initio* application of Gutzwiller correlations to a realistic electronic structure problem.

The plan of this article is as follows: in Sect. I we introduce the formalism of LDA+G starting from the constrained-search formulation of Density Functional Theory, demonstrating how the Gutzwiller wavefunction can be used to generalize LDA+U by allowing the expectation value of the atomic Hamiltonian to be computed on a multi-determinant wavefunction. In Sect. IB 1 and Sect. II we then show how the different terms of the LDA+G density functional can be computed by means of GA, and how the total energy of a correlated electronic system can be minimized by a three-step iterative procedure. In Sect. III we finally present and comment on the physical results for paramagnetic and ferromagnetic *bcc* Fe, and connect back to the basics questions about the origin of ferromagnetic order.

## I. CONSTRAINED-SEARCH FORMULATION OF A GUTZWILLER DENSITY FUNCTIONAL THEORY

A convenient way to introduce a Gutzwiller density functional is through the formalism independently proposed by Levy<sup>32,33</sup> and Lieb<sup>34</sup>. Starting from the Rayleigh-Ritz definition for the ground state energy  $E_{GS}$  of a system

$$E_{GS} = \min_{\Psi} \langle \Psi | \hat{H} | \Psi \rangle, \quad (1)$$

where the electron Hamiltonian  $\hat{H}$  includes the kinetic energy  $\hat{T}$ , the electron-electron interaction  $\hat{V}_{ee}$ , and a local external potential  $\hat{V}_{\text{ext}}$ , Levy and Lieb converted the variational principle for the ground state wavefunction into a variational principle for the ground state density through a constrained minimization at fixed density  $n(\mathbf{r})$

$$E_{\text{GS}}[V_{\text{ext}}(\mathbf{r})] = \min_{n(\mathbf{r})} \left\{ \min_{\Psi \rightarrow n(\mathbf{r})} \langle \Psi | \hat{T} + \hat{V}_{ee} | \Psi \rangle + \int V_{\text{ext}}(\mathbf{r}) n(\mathbf{r}) \right\}. \quad (2)$$

The first term on the right-hand side of (2) is nothing but the constrained-search definition of the Hohenberg-Kohn functional<sup>35</sup>, i.e.

$$F_{\text{HK}}[n(\mathbf{r})] = \min_{\Psi \rightarrow n(\mathbf{r})} \langle \Psi | \hat{T} + \hat{V}_{ee} | \Psi \rangle, \quad (3)$$

which is independent of the external potential  $V_{\text{ext}}$ . The wavefunction  $\Psi$  in the definition Eq. (3) should span the whole many-body Hilbert space, generally too large to allow a straightforward numerical evaluation of  $F_{\text{HK}}[n(\mathbf{r})]$ . Within the Kohn-Sham scheme, the generality of Eq. (3) is abandoned in favor of a more practical definition of the Hohenberg and Kohn functional, in which the latter is split into kinetic, Hartree, and exchange-correlation terms, namely

$$F_{\text{HK}}[n(\mathbf{r})] = T_s[n(\mathbf{r})] + E_{\text{H}}[n(\mathbf{r})] + E_{\text{xc}}[n(\mathbf{r})], \quad (4)$$

where  $E_{\text{H}}[n(\mathbf{r})]$  is simply the electrostatic energy of the electron density regarded as a classical charge distribution. A constrained search is then retained only for the kinetic contribution

$$T_s[n(\mathbf{r})] = \min_{\Psi \rightarrow n(\mathbf{r})} \langle \Psi | \hat{T} | \Psi \rangle, \quad (5)$$

which, because  $\hat{T}$  is a one-body operator, has a solution within the class of Slater determinants, a relatively simple task to accomplish through auxiliary non-interacting electron Hamiltonians whose ground state local density  $n(\mathbf{r})$  coincides with that of the physical interacting model. The insurmountable difficulties of the original many-body problem have thus been hidden in the unknown exchange-correlation functional  $E_{\text{xc}}[n(\mathbf{r})]$ . All DFT approximation schemes correspond just to different guesses of a physically sensible functional form of  $E_{\text{xc}}[n(\mathbf{r})]$  in terms of the local density.

The main problem that arises from the density-dependent parametrization Eq. (5) is that  $E_{\text{H}}[n(\mathbf{r})]$  contains a spurious self-interaction (SI) term – finite even when  $n(\mathbf{r})$  is the density of a single electron! – a term which should be identically cancelled in the exact  $E_{\text{xc}}[n(\mathbf{r})]$ . Unfortunately, all semi-local approximations to  $E_{\text{xc}}[n(\mathbf{r})]$ , such as LDA and Generalized Gradient Approximation (GGA), fail to fully subtract such a SI term from the density functional, which brings about

results that by construction contain a certain level of self-interaction error.

The spurious SI one-electron energy is larger for spatially localized electronic wavefunctions. For instance, a single electron with a simple gaussian wavefunction feels an SI that is inversely proportional to the standard deviation of the gaussian, only 70% of which is subtracted by the LDA exchange functional. The improvements attained by better functionals do not seem major.<sup>36</sup> All density-functional calculations are affected to some extent by the SI error, more important when the real-space density matrix is more localized. That is especially the case for most transition metals and transition-metal oxides. In a density functional calculation with semi-local functionals, the spurious SI term acts effectively as a penalty term preventing electronic localization, thus often spoiling agreement with experimental data for band gaps, magnetization, and other physical observables such as lattice constant and bulk modulus.

### A. LDA+U

A popular way to reduce the SI while still remaining in the context of local or semi-local density functionals is by including in the kinetic functional Eq. (5) also part of the electron-electron interaction, specifically the projection  $\hat{H}_{\text{at}}$  of  $\hat{V}_{ee}$  on atomic-like orbital (see below). The common choice is to consider only orbitals that are partially occupied within standard LDA, hence which suffer more from the SI. The non-interacting kinetic functional  $T_s[n(\mathbf{r})]$  is thus turned into a modified kinetic functional  $T_i[n(\mathbf{r})]$ :

$$T_s[n(\mathbf{r})] \rightarrow T_i[n(\mathbf{r})] = \min_{\Psi_0 \rightarrow n(\mathbf{r})} \langle \Psi_0 | \hat{T} + \hat{H}_{\text{at}} | \Psi_0 \rangle, \quad (6)$$

and the Hohenberg and Kohn functional changes into

$$F_{\text{HK}}[n(\mathbf{r})] = T_i[n(\mathbf{r})] + E_{\text{H}}[n(\mathbf{r})] + E_{\text{xc}}[n(\mathbf{r})] - E_{\text{dc}}[n(\mathbf{r})], \quad (7)$$

where  $E_{\text{dc}}[n(\mathbf{r})]$  is a double-counting energy which must cancel the contribution of  $\hat{H}_{\text{at}}$  already included within LDA.

In Eq. (6) the constrained-search is still restricted to the space of Slater-determinants  $\Psi_0$ , so that the modified kinetic functional can be dealt with within an independent-particle picture, and therefore included in the Kohn-Sham scheme. Essentially, the interaction  $\hat{H}_{\text{at}}$  is treated by Hartree-Fock, which is devoid of SI – while still unable to capture the Mott localization phenomenon, a correlation effect. In section IB we shall discuss how to improve the functional  $T_i$  so as to make Mott physics accessible. Here in addition we briefly discuss how to define properly  $\hat{H}_{\text{at}}$ . Typically  $\hat{H}_{\text{at}} = \sum_{\mathbf{R}} \hat{H}_{\text{at}}^{(\mathbf{R})}$ , with  $\hat{H}_{\text{at}}^{(\mathbf{R})}$  accounting for the leading order multipolar expansion of the Coulomb interaction projected onto a selected set of

atomic-like orbitals  $|\phi_{\mathbf{R},m}^{(l)}\rangle$  with angular momentum  $l$  at atomic site  $\mathbf{R}$  in the lattice,

$$\hat{H}_{\text{at}}^{(\mathbf{R})} = \frac{F_0}{2} \hat{N}_{\mathbf{R}} (\hat{N}_{\mathbf{R}} - 1) + \frac{1}{2} \sum_{L>0}^{2l} F_L (C_{l0L0}^{l0})^2 \sum_{M=-L}^L (-1)^M C_{lm'LM}^{lm} C_{lm'_1L-M}^{lm_1} c_{\mathbf{R},m\sigma}^\dagger c_{\mathbf{R},m_1\sigma_1}^\dagger c_{\mathbf{R},m'_1\sigma_1} c_{\mathbf{R},m'\sigma} \quad (8)$$

where  $\hat{N}_{\mathbf{R}}$  is the total electron number operator at site  $\mathbf{R}$  projected onto the selected set of atomic orbitals,  $L = 2n$  with  $n = 1, \dots, l$ , and  $C_{lm'LM}^{lm}$  are the Clebsch-Gordan coefficients. The parameters  $F_L$  are commonly known as Slater integrals. The first term on the right-hand side of Eq. (8), which we shall denote hereafter as  $\hat{H}_{\text{Hub}}^{(\mathbf{R})}$ , is a pure charge repulsion usually referred to as the Hubbard term, its coupling constant  $F_0$  generally called the "Hubbard  $U$ ". The remaining terms instead enforce Hund's first and second rules, hence they may be referred to as the Hund's rule exchange ( $\hat{H}_{\text{Hund}}$ ). In fact, in the case of  $p$  orbitals ( $l = 1$ ), the exact multipolar expansion can be rewritten solely in terms of the number operator  $\hat{N}_{\mathbf{R}}$ , the total spin  $\mathbf{S}_{\mathbf{R}}$  and total angular momentum  $\mathbf{L}_{\mathbf{R}}$  operators projected on the set  $|\phi_{\mathbf{R},m}^{(1)}\rangle$ :

$$\hat{H}_{\text{at}} = \frac{F_0}{2} \left[ \hat{N}_{\mathbf{R}} (\hat{N}_{\mathbf{R}} - 1) \right] + \frac{F_2}{2} \left[ \frac{4}{5} \hat{N}_{\mathbf{R}} - \frac{\hat{N}_{\mathbf{R}}^2}{5} - \frac{3}{25} \left( 4\hat{\mathbf{S}}_{\mathbf{R}} \cdot \hat{\mathbf{S}}_{\mathbf{R}} + \hat{\mathbf{L}}_{\mathbf{R}} \cdot \hat{\mathbf{L}}_{\mathbf{R}} \right) \right], \quad (9)$$

explicitly showing the content of the first two Hund rules. For  $l > 1$ , it is no longer possible to rewrite Eq. (8) in terms of simple operators like spin and angular momentum.

The well-known LDA+U method truncates the multipolar expansion of the Coulomb operator, Eq. (8), to the zeroth-order term, therefore setting  $\hat{H}_{\text{at}} = \hat{H}_{\text{Hub}}$ . With this recipe, the density dependence of the expectation value  $\langle \Psi_0 | \hat{H}_{\text{at}} | \Psi_0 \rangle$  can be written in terms of the matrix elements  $n_{lm\sigma\mathbf{R},lm'\sigma'\mathbf{R}}^{(0)} = \langle \Psi_0 | c_{\mathbf{R},lm\sigma}^\dagger c_{\mathbf{R},lm'\sigma'} | \Psi_0 \rangle$  of the local single-particle density matrix  $\hat{n}_{\mathbf{R}}^{(0)}$ , which is an implicit function of the density  $n(\mathbf{r})$ . If lattice periodicity is unbroken and the set of correlated orbitals is characterized by a single value of the angular momentum, we can drop both indices  $l$  and  $\mathbf{R}$  in any local operator, and write  $\hat{n}_{\mathbf{R}}^{(0)} = \hat{n}^{(0)}$ ,  $\forall \mathbf{R}$ . The double-counting correction  $E_{\text{dc}}[n(\mathbf{r})]$  in LDA+U is commonly chosen so as to cancel  $\langle \Psi_0 | \hat{H}_{\text{at}} | \Psi_0 \rangle$  in the limiting case of an idempotent single-particle density matrix  $\hat{n}^{(0)}$ ,<sup>37</sup> which corresponds to assuming that, within straight LDA,  $\langle \hat{n}_{\mathbf{R}}^{(0)} \hat{n}_{\mathbf{R}}^{(0)} \rangle = \langle \hat{n}_{\mathbf{R}}^{(0)} \rangle \langle \hat{n}_{\mathbf{R}}^{(0)} \rangle$ . With this assumption, the  $U$ -dependent part of Kohn-Sham Hamiltonian is equal to the positive definite contribution

$$\langle \Psi_0 | \hat{H}_{\text{at}} | \Psi_0 \rangle - E_{\text{dc}}[n(\mathbf{r})] = \frac{U}{2} \text{Tr} \left[ \hat{n}^{(0)} (1 - \hat{n}^{(0)}) \right]. \quad (10)$$

An optimal value of  $U$  can be estimated by linear response calculations<sup>38,39</sup>, or empirically determined by agreement with experimental data.

The advantage of using Eq. (10) to improve the description of systems with strongly localized electrons is both its simplicity, involving no further computational effort than that needed to solve the Kohn-Sham equations, and its success in removing the self-interaction whenever  $U$  is sensibly chosen. However, there are of course situations in which the empirical LDA+U functional will not be adequate. We previously mentioned that Mott localization because of its genuinely many-body, collective nature, is not accessible by LDA+U nor by any other technique that relies on a single-particle description. Moreover, it is well known that only the spherically-averaged strength of the exchange-correlation hole is correctly accounted for by the LDA functional, but not its angular dependence. For these reasons one cannot expect that LDA+U will be apt to describe systems that display strongly orbital-dependent correlations, as was shown to be the case of body-centered cubic iron.<sup>27</sup> Indeed recent studies on iron pnictides and chalcogenides<sup>40-42</sup> suggest that the orbital selectivity displayed by these iron compounds crucially depends on atomic Hund's rules. These observations indicate that a way to further improve LDA beyond LDA+U will not only be the inclusion of correlations in the modified kinetic functional so as to make Mott localization accessible, but also the introduction of an appropriate expression for Hund's interaction  $\hat{H}_{\text{Hund}}$  in the atomic Hamiltonian  $\hat{H}_{\text{at}}$ , so as to account for orbital selectivity. However, when Hund's rule exchange, the second term in the r.h.s. of Eq. (8), is taken into account, one faces the problem of finding a proper expression for electron double counting. The latter should by definition be equivalent to the LDA approximation to the atomic interaction energy, Eq. (8). However, that average depends in principle on the specific point symmetry of the system, and one cannot find a general expression valid for every case. The conventional way to proceed is to dismiss the hope of including within LDA+U the whole atomic interaction Eq. (8), and instead be content with only terms that depend on angular-averaged local operators, specifically the total number operator  $\hat{N}_{\mathbf{R}}$  and total spin  $\hat{\mathbf{S}}_{\mathbf{R}}$ . These terms are identified by noting that, using the re-coupling formula

$$\sum_M (-1)^M C_{lm'LM}^{lm} C_{lm'_1L-M}^{lm_1} = \sum_{\Lambda\lambda} (2\Lambda + 1) \left\{ \begin{matrix} L & l & l \\ \Lambda & l & l \end{matrix} \right\} (-1)^{L+\Lambda} (-1)^\lambda C_{lm'_1\Lambda\lambda}^{lm} C_{lm'\Lambda-\lambda}^{lm_1},$$

the  $L > 0$  contribution of Eq. (8) can be also written as

$$\begin{aligned} \hat{H}_{\text{at } L>0}^{(\mathbf{R})} &= -\frac{1}{2} \sum_{mm_1m'm'_1} \sum_{\sigma\sigma_1} \sum_{L>0}^{2l} F_L (C_{l_0 L_0}^{l_0})^2 \\ &\sum_{\Lambda} \sum_{\lambda=-\Lambda}^{\Lambda} (-1)^{\Lambda+\lambda} (2\Lambda+1) \left\{ \begin{matrix} L & l & l \\ \Lambda & l & l \end{matrix} \right\} \\ &C_{lm'_1}^{lm} C_{lm'_1}^{lm_1} C_{lm\sigma}^\dagger C_{lm'_1\sigma_1}^\dagger C_{lm_1\sigma_1} C_{lm'\sigma}, \end{aligned}$$

where  $\{ \dots \}$  denote the Wigner  $6j$ -symbols. We can then select out the term with  $\Lambda = 0$ , which depends on rotationally invariant densities, re-couple back  $m$  with  $m'$  and  $m_1$  with  $m'_1$  in the remaining terms, and iterate the procedure. At the end, we obtain a term that involves rotationally invariant densities, plus another interaction that cannot be expressed by any means in terms of those densities. The former together with the Hubbard  $U$  define the part of the atomic interaction Eq. (8) easier to implement within LDA+U, namely

$$\begin{aligned} \hat{H}_{\text{at}}^{(\mathbf{R})} &\simeq \frac{U}{2} \hat{N}_{\mathbf{R}} (\hat{N}_{\mathbf{R}} - 1) - \frac{2l+1}{2l+2} J \left[ \hat{\mathbf{S}}_{\mathbf{R}} \cdot \hat{\mathbf{S}}_{\mathbf{R}} - \frac{3}{4} \hat{N}_{\mathbf{R}} \right. \\ &\left. + \frac{\hat{N}_{\mathbf{R}} (\hat{N}_{\mathbf{R}} - 1)}{4} + \frac{\hat{N}_{\mathbf{R}} (\hat{N}_{\mathbf{R}} - 1)}{2(2l+1)} \right], \end{aligned} \quad (11)$$

where  $J$  is conventionally defined as<sup>38,39</sup>

$$J = \frac{1}{2l} \sum_{L>0}^{2l} (C_{l_0 L_0}^{l_0})^2 F_L, \quad (12)$$

which, for  $d$ -orbitals, i.e.  $l = 2$ , is  $J = (F_0 + F_4)/14$ . The double counting term associated with Eq. (11) is obtained analogously as before and reads in the general case of a spin-polarized calculation

$$\begin{aligned} E_{\text{dc}} &= \frac{U}{2} N(N-1) - \frac{2l+1}{4l+4} J \left[ N_{\uparrow} (N_{\uparrow} - 1) \right. \\ &\left. + N_{\downarrow} (N_{\downarrow} - 1) + \frac{N(N-1)}{2l+2} \right]. \end{aligned} \quad (13)$$

The expression (11) can be further simplified to get rid of the  $l$  dependence, by reabsorbing the  $l$  in the definition of  $J$ , and by adopting a simplified version of the last term in square brackets, leading to the following results

$$\hat{H}_{\text{Hund}} = -J \left\{ \hat{S}^2 - \frac{3}{4} \hat{N} + \frac{\hat{N}(\hat{N}-1)}{4} + \sum_m \hat{n}_{m\uparrow} \hat{n}_{m\downarrow} \right\}. \quad (14)$$

for which we choose a double-counting energy of the type

$$\begin{aligned} E_{\text{dc}}^{\text{Hund}}[n(\mathbf{r})] &= \\ &= -J \left[ \frac{N_{\uparrow}(N_{\uparrow}-1)}{2} + \frac{N_{\downarrow}(N_{\downarrow}-1)}{2} + \frac{N_{\uparrow}N_{\downarrow}}{2l+1} \right]. \end{aligned} \quad (15)$$

## B. Extending LDA+U to LDA+Gutzwiller

The key difference between LDA+G and LDA+U resides in the definition of the modified kinetic functional  $T_i$ . Within LDA+G, the definition Eq. (6) changes to

$$T_i[n(\mathbf{r})] \rightarrow T_G[n(\mathbf{r})] = \min_{\Psi_G \rightarrow n(\mathbf{r})} \langle \Psi_G | \hat{T} + \hat{H}_{\text{at}} | \Psi_G \rangle, \quad (16)$$

where the wavefunction  $|\Psi_G\rangle$  is defined as

$$|\Psi_G\rangle = \hat{\mathcal{P}} |\Psi_0\rangle = \prod_{\mathbf{R}} \hat{\mathcal{P}}_{\mathbf{R}} |\Psi_0\rangle. \quad (17)$$

In the above equation,  $|\Psi_0\rangle$  is still a Slater determinant, and the elements of novelty are the operators  $\hat{\mathcal{P}}_{\mathbf{R}}$ , which are linear transformations acting on the configurational space of a chosen set of local orbitals at lattice site  $\mathbf{R}$ . As in LDA+U, this set of orbitals  $\phi_{m,\mathbf{R}}$  retain well defined atomic angular momentum  $l$ ,  $m$  being its projection on a given quantization axis. The operator  $\hat{\mathcal{P}}_{\mathbf{R}}$  can be generally written as

$$\hat{\mathcal{P}}_{\mathbf{R}} = \sum_{\Gamma'} \Lambda_{\Gamma\Gamma',\mathbf{R}} |\Gamma, \mathbf{R}\rangle \langle \Gamma', \mathbf{R}|, \quad (18)$$

where  $|\Gamma, \mathbf{R}\rangle$  denote many-body configurations of electrons occupying the orbitals  $\phi_{m,\mathbf{R}}$ . Differently from LDA+U, the expectation value of the kinetic plus atomic interaction operators will not depend solely on the Slater determinant  $|\Psi_0\rangle$ , but also on the variational parameters  $\Lambda_{\Gamma\Gamma',\mathbf{R}}$  that define  $\hat{\mathcal{P}}_{\mathbf{R}}$ .

Computing exact expectation values on the Gutzwiller wavefunction for lattices of finite coordination is a task that can be accomplished only numerically, e.g. through Variational Quantum Monte Carlo.<sup>11,43</sup> For infinite-coordination lattices, an exact expression can be instead computed analytically. There is in fact a close connection between the Gutzwiller variational approach in the limit of infinite lattice coordination and dynamical mean field theory.<sup>6</sup> In that limit, the single particle self-energy matrix  $\Sigma(\epsilon, \mathbf{k}) = \Sigma(\epsilon)$  becomes purely local, hence momentum independent. DMFT allows to evaluate exactly  $\Sigma(\epsilon)$  by solving an auxiliary Anderson impurity model constructed in such a way as to have the same self-energy. The Gutzwiller variational approach is instead a consistent approximation to the exact solution, which assumes a Fermi-liquid expression  $\Sigma(\epsilon) \simeq \Sigma(0) + (1 - Z^{-1})\epsilon$ , where  $Z$  is commonly referred to as the quasiparticle weight. Because of this assumption, the Gutzwiller wavefunction can describe only states whose elementary excitations are quasiparticles, such as Landau-Fermi liquids and insulators that can be represented through a Slater determinant. However, the additional freedom brought by the parameter  $Z$ , whose value is strictly  $Z = 1$  within Hartree-Fock and in LDA+U, opens the possibility to access strongly correlated metals,  $Z \ll 1$ , and thus the approach to a Mott transition, where  $Z \rightarrow 0$ . Although DMFT is exact only in the limit of infinite coordination,

it is currently used as an approximation in realistic finite-coordination lattices, under the hypothesis that (strong) correlation effects beyond Hartree-Fock (HF) are well represented by  $\Sigma(\epsilon, \mathbf{k}) \simeq \Sigma_{\text{HF}}(\mathbf{k}) + \Sigma(\epsilon)$ , where  $\Sigma_{\text{HF}}(\mathbf{k})$  is the HF self-energy, eventually including frequency-dependent random-phase-like contributions,<sup>44</sup> and the correction  $\Sigma(\epsilon)$  is momentum independent and can be obtained by DMFT. Under the same assumptions, one can keep using the formal results of the Gutzwiller variational approach, that are strictly valid only in infinite-coordination lattices, also in finite-coordination ones, an approximation referred to as the *Gutzwiller approximation* (GA). In other words, the GA should be better regarded as an approximation to DMFT, when either of them are used in finite-coordination lattices, rather than an approximation to the exact evaluation of average values on the Gutzwiller wavefunction, Eq. (17). This viewpoint, which we underwrite, is our motivation for adopting the Gutzwiller approximation in combination with LDA+U as an alternative to LDA+DMFT, at the cost of less rigor, but as we shall show with gain in simplicity and flexibility.

### 1. Expectation values in the Gutzwiller Approximation

In order to determine the functional  $T_G[n(\mathbf{r})]$ , one should be able to compute expectation values of both many-body on-site operators such as those contained in  $\hat{H}_{\text{at}}$ , and off-site single-particle operators, which are present in the definition of the kinetic operator  $\hat{T}$ . In all what follows, we shall use the formalism presented in Ref. 45.

First of all, the Slater determinant  $|\Psi_0\rangle$  defines the uncorrelated one-body local density-matrix  $\hat{n}_{\mathbf{R}}^{(0)}$  (the same matrix that enters the LDA+U energy correction term Eq. (10)), with elements

$$n_{\mathbf{R}m\sigma, \mathbf{R}m'\sigma'}^{(0)} = \langle \Psi_0 | c_{\mathbf{R},m\sigma}^\dagger c_{\mathbf{R},m'\sigma'} | \Psi_0 \rangle, \quad (19)$$

where  $c_{\mathbf{R},m\sigma}^\dagger$  creates a spin- $\sigma$  electron in orbital  $\phi_{m,\mathbf{R}}$ .  $\hat{n}_{\mathbf{R}}^{(0)}$  is diagonalized by a unitary transformation that turns the original basis of operators  $c_{\mathbf{R},m\sigma}^\dagger$  into the natural basis of operators  $c_{\mathbf{R},\gamma\sigma}^\dagger$ , assuming invariance with respect to spin rotations around the  $z$ -axis. In the natural basis, the one-body density matrix is therefore diagonal, with eigenvalues  $n_{\mathbf{R},\gamma\sigma}^{(0)}$ . In the natural-orbital Fock basis, with states

$$|\{n_{\mathbf{R},\gamma\sigma}\}\rangle \equiv \prod_{\gamma\sigma} \left( c_{\mathbf{R},\gamma\sigma}^\dagger \right)^{n_{\mathbf{R},\gamma\sigma}} |0\rangle,$$

it follows that the probability matrix

$$\begin{aligned} P_{0, \{n_{\mathbf{R},\gamma\sigma}\} \{m_{\mathbf{R},\gamma\sigma}\}}^{(\mathbf{R})} &\equiv \langle \Psi_0 | \{m_{\mathbf{R},\gamma\sigma}\} \langle \{n_{\mathbf{R},\gamma\sigma}\} | \Psi_0 \rangle \\ &= P_{0, \{n_{\mathbf{R},\gamma\sigma}\}}^{(\mathbf{R})} \delta_{\{n_{\mathbf{R},\gamma\sigma}\} \{m_{\mathbf{R},\gamma\sigma}\}} \\ &= \prod_{\gamma\sigma} \left( n_{\mathbf{R},\gamma\sigma}^{(0)} \right)^{n_{\mathbf{R},\gamma\sigma}} \left( 1 - n_{\mathbf{R},\gamma\sigma}^{(0)} \right)^{1-n_{\mathbf{R},\gamma\sigma}}, \quad (20) \end{aligned}$$

is diagonal, too. It is actually convenient<sup>45</sup> to rewrite the operator Eq. (18) in a mixed basis representation as

$$\hat{P}_{\mathbf{R}} = \sum_{\Gamma \{n_{\mathbf{R},\gamma\sigma}\}} \left( \frac{\Phi_{\Gamma \{n_{\mathbf{R},\gamma\sigma}\}, \mathbf{R}}}{P_{0, \{n_{\mathbf{R},\gamma\sigma}\}}^{(\mathbf{R})}} \right) |\Gamma, \mathbf{R}\rangle \langle \{n_{\mathbf{R},\gamma\sigma}\}|, \quad (21)$$

where  $|\Gamma, \mathbf{R}\rangle$  is a state, e.g. a Fock state, in the original basis, whereas  $|\{n_{\mathbf{R},\gamma\sigma}\}\rangle$  is a Fock state in the natural basis. This mixed representation simplifies considerably the calculations. In order to use the Gutzwiller approximation, we need to impose the two following constraints on the matrix  $\hat{\Phi}_{\mathbf{R}}$  with elements  $\Phi_{\Gamma \{n_{\mathbf{R},\gamma\sigma}\}, \mathbf{R}}$ :<sup>45</sup>

$$\text{Tr} \left\{ \hat{\Phi}_{\mathbf{R}}^\dagger \hat{\Phi}_{\mathbf{R}} \right\} = 1, \quad (22)$$

$$\text{Tr} \left\{ \hat{\Phi}_{\mathbf{R}}^\dagger \hat{\Phi}_{\mathbf{R}} \hat{c}_{\mathbf{R},\gamma\sigma}^\dagger \hat{c}_{\mathbf{R},\gamma'\sigma'} \right\} = n_{\mathbf{R},\gamma\sigma}^{(0)} \delta_{\gamma\gamma'} \delta_{\sigma\sigma'}, \quad (23)$$

where  $\hat{c}_{\mathbf{R},\gamma\sigma}^\dagger$  is the matrix representation of the Fermi operator in its Fock basis. If these constraints are fulfilled, then within the Gutzwiller approximation, which we recall is exact for infinite-coordination lattices, we have

$$\langle \Psi_G | \hat{O}_{\mathbf{R}} | \Psi_G \rangle = \text{Tr} \left\{ \hat{\Phi}_{\mathbf{R}}^\dagger \hat{O}_{\mathbf{R}} \hat{\Phi}_{\mathbf{R}} \right\}, \quad (24)$$

where  $\hat{O}_{\mathbf{R}}$  is the matrix representation of any local operator. The inter-site density matrix can be computed from

$$\begin{aligned} \langle \Psi_G | \hat{c}_{\mathbf{R},m\sigma}^\dagger \hat{c}_{\mathbf{R},m'\sigma'} | \Psi_G \rangle &= \sum_{\gamma\gamma'} R_{\gamma m, \sigma, \mathbf{R}}^\dagger R_{m' \gamma', \sigma', \mathbf{R}} \\ &\langle \Psi_0 | c_{\mathbf{R},\gamma\sigma}^\dagger c_{\mathbf{R},\gamma'\sigma'} | \Psi_0 \rangle, \quad (25) \end{aligned}$$

where

$$R_{\gamma m, \sigma, \mathbf{R}}^\dagger = \frac{\text{Tr} \left\{ \hat{\Phi}_{\mathbf{R}}^\dagger \hat{c}_{\mathbf{R},m\sigma}^\dagger \hat{\Phi}_{\mathbf{R}} \hat{c}_{\mathbf{R},\gamma\sigma} \right\}}{\sqrt{n_{\mathbf{R},\gamma\sigma}^{(0)} (1 - n_{\mathbf{R},\gamma\sigma}^{(0)})}}, \quad (26)$$

can be regarded as a wavefunction renormalization matrix. Here  $\hat{c}_{\mathbf{R},m\sigma}^\dagger$  is the matrix representation of the original operators in the basis of states  $|\Gamma, \mathbf{R}\rangle$ . When this is the Fock basis constructed by the same original operators, their matrix representation is actually independent of the basis of single-particle wavefunctions which they refer to, hence it is the same as for the  $\hat{c}_{\mathbf{R},\gamma\sigma}^\dagger$  operators of the natural basis. In reality, in most cases that are relevant for real materials the natural basis that diagonalizes the local density matrix is determined fully by

the lattice symmetry, hence it is possible and convenient to write the Hamiltonian directly in that basis. In the above formulas, this corresponds to identifying the set of labels  $\{m\}$  with  $\{\gamma\}$ . Since the natural basis is such both for the uncorrelated on-site density matrix

$$\begin{aligned} n_{\mathbf{R}m\sigma,m'\sigma'}^{(0)} &= \langle \Psi_0 | \hat{c}_{\mathbf{R},m\sigma}^\dagger \hat{c}_{\mathbf{R},m'\sigma'} | \Psi_0 \rangle \\ &= \text{Tr} \left\{ \hat{\Phi}_{\mathbf{R}}^\dagger \hat{\Phi}_{\mathbf{R}} \hat{c}_{\mathbf{R},m\sigma}^\dagger \hat{c}_{\mathbf{R},m'\sigma'} \right\} \\ &= \delta_{mm'} n_{\mathbf{R},m\sigma}^{(0)}, \end{aligned} \quad (27)$$

and for the correlated one

$$\begin{aligned} n_{\mathbf{R}m\sigma,m'\sigma'} &= \langle \Psi_G | \hat{c}_{\mathbf{R},m\sigma}^\dagger \hat{c}_{\mathbf{R},m'\sigma'} | \Psi_G \rangle \\ &= \text{Tr} \left\{ \hat{\Phi}_{\mathbf{R}}^\dagger \hat{c}_{\mathbf{R},m\sigma}^\dagger \hat{c}_{\mathbf{R},m'\sigma'} \hat{\Phi}_{\mathbf{R}} \right\} \\ &= \delta_{mm'} n_{\mathbf{R},m\sigma}, \end{aligned} \quad (28)$$

generally with different eigenvalues, it is not difficult to realize that the wavefunction renormalization matrix Eq. (26) becomes diagonal, i.e.

$$R_{m'm,\sigma,\mathbf{R}}^\dagger = \frac{\text{Tr} \left\{ \hat{\Phi}_{\mathbf{R}}^\dagger \hat{c}_{\mathbf{R},m\sigma}^\dagger \hat{\Phi}_{\mathbf{R}} \hat{c}_{\mathbf{R},m'\sigma} \right\}}{\sqrt{n_{\mathbf{R},m'\sigma}^{(0)}(1 - n_{\mathbf{R},m'\sigma}^{(0)})}} = \delta_{mm'} R_{m\sigma,\mathbf{R}}^\dagger. \quad (29)$$

The Eqs. (24)–(29) are the basic formulas that allow to evaluate the average value of the Hamiltonian as a functional of the Slater determinant and of the matrices  $\hat{\Phi}_{\mathbf{R}}$ , hence to solve the variational problem.

## II. THE GUTZWILLER FUNCTIONAL IN PRACTICE

In this section we show how to perform a density-self-consistent LDA+G calculation on a realistic system, namely *bcc* Fe which, as mentioned in the Introduction, although a basic and supposedly simple system, still exhibits controversial aspects.

We first have to select the *correlated* orbitals to be treated by the Gutzwiller operator. In the present case the choice is simple: the *3d* orbitals of Fe. This case is one of those mentioned earlier in which the natural basis is determined by symmetry and corresponds to the cubic crystal field split *d* orbitals, namely the  $e_g$  doublet and the  $t_{2g}$  triplet. In this representation the formulas Eqs. (27)–(29) hold, which is a great simplification. Furthermore, since *bcc* is a Bravais lattice, the positions  $\mathbf{R}$  of Fe atoms also label unit cells, hence by translational symmetry we can safely assume that the variational matrix parameters  $\hat{\Phi}_{\mathbf{R}} = \hat{\Phi}$  are independent of  $\mathbf{R}$ . So are therefore the eigenvalues of the local density matrices,  $n_{\mathbf{R},m\sigma}^{(0)} = n_{m\sigma}^{(0)}$  and  $n_{\mathbf{R},m\sigma} = n_{m\sigma}$ , as well as the wavefunction renormalization  $R_{m\sigma,\mathbf{R}} = R_{m\sigma}$ . To lighten notations, in what follows the orbital labels  $m$  will refer both to the correlated set and to the uncorrelated ones,

unaffected by the action of the Gutzwiller operator. In the last paragraph of this section we shall come back to this point.

We define the Gutzwiller density functional as

$$\mathcal{F}[n(\mathbf{r})] = \min_{\Psi_G \rightarrow n(\mathbf{r})} \mathcal{E}[\Psi_G, n(\mathbf{r})]. \quad (30)$$

where the quantity  $\mathcal{E}[\Psi_G, n(\mathbf{r})]$  undergoing constrained minimization is

$$\begin{aligned} \mathcal{E}[\Psi_G, n(\mathbf{r})] &= \langle \Psi_G | \hat{T} + \hat{H}_{\text{int}} | \Psi_G \rangle + \\ &+ \int V_{\text{ext}}(\mathbf{r})n(\mathbf{r})d\mathbf{r} + \tilde{E}_{\text{H}}[n(\mathbf{r})] + \tilde{E}_{\text{xc}}[n(\mathbf{r})] - E_{\text{dc}}[n(\mathbf{r})]. \end{aligned} \quad (31)$$

For our purposes, it is convenient to rewrite Eq. (30) as a minimization constrained with respect to the ‘‘uncorrelated’’ density  $n^{(0)}(\mathbf{r})$ ,

$$\mathcal{F}[n^{(0)}(\mathbf{r})] = \min_{\hat{\mathcal{P}}, \Psi_0 \rightarrow n^{(0)}(\mathbf{r})} \mathcal{E}[\Psi_0, \hat{\mathcal{P}}, n^{(0)}(\mathbf{r})], \quad (32)$$

where  $\mathcal{E}[\Psi_0, \hat{\mathcal{P}}, n^{(0)}(\mathbf{r})] = \mathcal{E}[\Psi_G(\Psi_0, \hat{\mathcal{P}}), n(\Psi_0, \hat{\mathcal{P}})]$ . The dependence of the ‘‘correlated’’ density  $n(\mathbf{r})$  upon the ‘‘uncorrelated’’ density  $n^{(0)}(\mathbf{r})$  can be made explicit once one writes them in terms of the one-body ‘‘correlated’’ density-matrix of the periodic system

$$D_{mm',\sigma,\mathbf{R}} = \langle \Psi_G | \hat{c}_{\mathbf{R},m\sigma}^\dagger \hat{c}_{\mathbf{0},m'\sigma} | \Psi_G \rangle, \quad (33)$$

and of the ‘‘uncorrelated’’ density-matrix

$$D_{mm',\sigma,\mathbf{R}}^{(0)} = \langle \Psi_0 | \hat{c}_{\mathbf{R},m\sigma}^\dagger \hat{c}_{\mathbf{0},m'\sigma} | \Psi_0 \rangle, \quad (34)$$

namely

$$\begin{aligned} n^{(0)}(\mathbf{r}) &= \sum_{\sigma} n_{\sigma}^{(0)}(\mathbf{r}) \\ &= \sum_{m,m',\sigma,\mathbf{R}} D_{mm',\sigma,\mathbf{R}}^{(0)} \phi_{m,\mathbf{R}}^*(\mathbf{r}) \phi_{m',\mathbf{0}}(\mathbf{r}), \end{aligned} \quad (35)$$

$$\begin{aligned} n(\mathbf{r}) &= \sum_{\sigma} n_{\sigma}(\mathbf{r}) \\ &= \sum_{m,m',\sigma,\mathbf{R}} D_{mm',\sigma,\mathbf{R}} \phi_{m,\mathbf{R}}^*(\mathbf{r}) \phi_{m',\mathbf{0}}(\mathbf{r}). \end{aligned} \quad (36)$$

Indeed,  $D_{mm',\sigma,\mathbf{R}}$  can be obtained by  $D_{mm',\sigma,\mathbf{R}}^{(0)}$  using the recipe of the Gutzwiller Approximation:

$$D_{mm',\sigma,\mathbf{R}} = \begin{cases} R_{m\sigma}^\dagger D_{mm',\sigma,\mathbf{R}}^{(0)} R_{m'\sigma}, & \mathbf{R} \neq \mathbf{0}, \\ \text{Tr} \left\{ \hat{\Phi}^\dagger \hat{n}_{mm',\sigma} \hat{\Phi} \right\} = \delta_{mm'} n_{m\sigma}, & \mathbf{R} = \mathbf{0}, \end{cases} \quad (37)$$

where  $\hat{n}_{mm',\sigma}$  is the matrix representation on the local Fock space at site  $\mathbf{R}$  of  $\hat{c}_{\mathbf{R},m\sigma}^\dagger \hat{c}_{\mathbf{R},m'\sigma}$ , which is independent of  $\mathbf{R}$  for a periodic system, and where  $n_{m\sigma}$  is equal to  $n_{\mathbf{R}=\mathbf{0},m\sigma}$  defined in Eq. (28).

In order to write  $\mathcal{E}[\Psi_0, \hat{\mathcal{P}}, n^{(0)}(\mathbf{r})]$  explicitly in terms of the new variables, we start from the first and second terms of Eq. (31). We can now treat the kinetic and the external potential terms on the same footing through

$$\begin{aligned} \langle \Psi_G | \hat{T} | \Psi_G \rangle + \int n(\mathbf{r}) V_{\text{ext}}(\mathbf{r}) d\mathbf{r} = \\ \sum_{m, m', \sigma, \mathbf{R}} \left( T_{mm', \mathbf{R}} + V_{mm', \mathbf{R}}^{(\text{ext})} \right) D_{mm', \sigma, \mathbf{R}}, \end{aligned} \quad (38)$$

where values of  $T_{mm', \mathbf{R}}$  and  $V_{mm', \mathbf{R}}^{(\text{ext})}$  are the spin-independent matrix elements of the kinetic and external potential operators computed between our basis orbitals at sites  $\mathbf{R}$  and  $\mathbf{0}$ , i.e.

$$V_{mm', \mathbf{R}}^{(\text{ext})} = \int \phi_{m, \mathbf{R}}^*(\mathbf{r}) V_{\text{ext}}(\mathbf{r}) \phi_{m', \mathbf{0}}(\mathbf{r}) d\mathbf{r}, \quad (39)$$

$$T_{mm', \mathbf{R}} = -\frac{\hbar^2}{2m} \int \phi_{m, \mathbf{R}}^*(\mathbf{r}) \left[ \nabla^2 \phi_{m', \mathbf{0}}(\mathbf{r}) \right] d\mathbf{r} \quad (40)$$

and compute the value of the atomic interaction energy  $\langle \Psi_G | \hat{H}_{\text{at}} | \Psi_G \rangle$  using the Gutzwiller Approximation recipe

$$E_{\text{at}}[\Psi_0, \hat{\mathcal{P}}] = \langle \Psi_G | \hat{H}_{\text{at}} | \Psi_G \rangle = \text{Tr} \left\{ \hat{\Phi}^\dagger \hat{H}_{\text{at}} \hat{\Phi} \right\} \quad (41)$$

In order to simplify the density self-consistent LDA+G minimization we decided to use the Hartree  $\tilde{E}_{\text{H}}[n(\mathbf{r})]$  and exchange-correlation  $\tilde{E}_{\text{xc}}[n(\mathbf{r})]$  functionals as the LDA functionals linearized around the uncorrelated density  $n^{(0)}(\mathbf{r})$ . We checked *a posteriori* the accuracy of such a linearization. The modified Hartree functional then reads

$$\begin{aligned} \tilde{E}_{\text{H}} \left[ n^{(0)}(\mathbf{r}), n(\mathbf{r}) \right] \simeq \frac{e^2}{2} \int d\mathbf{r} d\mathbf{r}' \frac{n^{(0)}(\mathbf{r}) n^{(0)}(\mathbf{r}')}{|\mathbf{r} - \mathbf{r}'|} \\ + \int d\mathbf{r} \delta n(\mathbf{r}) v_{\text{H}}[n^{(0)}(\mathbf{r})], \end{aligned} \quad (42)$$

where  $\delta n(\mathbf{r}) = \sum_{\sigma} \delta n_{\sigma}(\mathbf{r}) = \sum_{\sigma} n_{\sigma}(\mathbf{r}) - n^{(0)}(\mathbf{r})$  and  $v_{\text{H}}[n^{(0)}(\mathbf{r})]$  is the conventional Hartree potential, whereas the exchange-correlation functional is

$$\begin{aligned} \tilde{E}_{\text{xc}} \left[ n^{(0)}(\mathbf{r}), n(\mathbf{r}) \right] = \sum_{\sigma} \int d\mathbf{r} n_{\sigma}^{(0)}(\mathbf{r}) \epsilon_{\text{xc}, \sigma}[n^{(0)}(\mathbf{r})] \\ + \int d\mathbf{r} v_{\text{xc}, \sigma}[n^{(0)}(\mathbf{r})] \delta n_{\sigma}(\mathbf{r}), \end{aligned} \quad (43)$$

$v_{\text{xc}}[n^{(0)}(\mathbf{r})]$  being the LDA exchange-correlation potential. Note that the choice of  $\tilde{E}_{\text{H}}$  involves neglecting a

term

$$\begin{aligned} \Delta E_{\text{H}} \left[ n^{(0)}(\mathbf{r}), n(\mathbf{r}) \right] &= \tilde{E}_{\text{H}} \left[ n^{(0)}(\mathbf{r}), n(\mathbf{r}) \right] - E_{\text{H}}[n(\mathbf{r})] = \\ &= \frac{e^2}{2} \int d\mathbf{r} d\mathbf{r}' \frac{\delta n(\mathbf{r}) \delta n(\mathbf{r}')}{|\mathbf{r} - \mathbf{r}'|} \end{aligned} \quad (44)$$

which can be interpreted as the energy of correlation-induced charge fluctuations. This term, together with the corresponding one neglected for the exchange-correlation functional,  $\Delta E_{\text{xc}} \left[ n^{(0)}(\mathbf{r}), n(\mathbf{r}) \right]$ , can be computed at the end of the LDA+G calculation in order to provide an estimate of the error due to approximations (42) and (43) (see Table VI). It is worth mentioning that the linearization (43) of exchange-correlation energy around the ‘‘uncorrelated’’ density does not spoil the sum rule for the LDA exchange-correlation hole. As for the double-counting term, similarly to what is done within LDA+U, it is chosen as a function of the local ‘‘uncorrelated’’ density-matrix  $n^{(0)}$  only,  $E_{\text{dc}}[n(\mathbf{r})] = E_{\text{dc}}[n^{(0)}]$ . In Sect. III we take as its explicit form the one of Eq. (13), having chosen our atomic interaction Hamiltonian  $\hat{H}_{\text{at}}$  to be the expression of Eq. (11).

### A. Three-step minimization of the LDA+Gutzwiller functional

The two densities  $n(\mathbf{r})$  and  $n^{(0)}(\mathbf{r})$  must be such that Gutzwiller constraints are fulfilled. In our case where original and natural basis coincide, the constraints on the density matrix can be written as

$$D_{mm', \sigma, \mathbf{R}=\mathbf{0}}^{(0)} = n_{m\sigma}^{(0)} \delta_{mm'}, \quad (45)$$

$$\text{Tr} \left\{ \hat{\Phi}^\dagger \hat{\Phi} \hat{n}_{mm', \sigma} \right\} = n_{m\sigma}^{(0)} \delta_{mm'}, \quad (46)$$

where we regard  $n_{m\sigma}^{(0)}$  as an additional independent variational parameter of the density functional. These constraints can be enforced with Lagrange multipliers, together with the first Gutzwiller constraint

$$\text{Tr} \left\{ \hat{\Phi}^\dagger \hat{\Phi} \right\} = 1. \quad (47)$$

Summing up all contributions and adding the electrostatic ion-ion interaction  $E_{\text{ion}}$ , we find that the overall functional we need to minimize has the form

$$\begin{aligned}
\mathcal{F}[n(\mathbf{r}), n^{(0)}(\mathbf{r}), n_{m\sigma}^{(0)}] &= \max_{\lambda\lambda'\lambda_0} \left[ \mathcal{K}[n(\mathbf{r})] + E_{\text{at}}[n(\mathbf{r})] - E_{\text{dc}}[n_{m\sigma}^{(0)}] + E_{\text{H}}^{(0)}[n^{(0)}(\mathbf{r})] + E_{\text{xc}}^{(0)}[n^{(0)}(\mathbf{r})] - \lambda_0 \left( \text{Tr} \left\{ \hat{\Phi}^\dagger \hat{\Phi} \right\} - 1 \right) \right. \\
&\quad \left. - \sum_{mm'\sigma} \lambda'_{mm',\sigma} \left( D_{mm',\sigma,\mathbf{R}=0}^{(0)} - n_{m\sigma}^{(0)} \delta_{mm'} \right) - \lambda_{mm',\sigma} \left( \text{Tr} \left\{ \hat{\Phi}^\dagger \hat{\Phi} \hat{n}_{mm',\sigma} \right\} - n_{m\sigma}^{(0)} \delta_{mm'} \right) \right] + E_{\text{ion}}, \quad (48)
\end{aligned}$$

where the functional  $\mathcal{K}[n(\mathbf{r})]$  contains all terms which depend on  $n(\mathbf{r})$  linearly through the renormalized density matrix  $D$ , namely

$$\begin{aligned}
\mathcal{K}(D) &= \sum_{mm',\sigma,\mathbf{R}} \left[ T_{mm',\mathbf{R}} + V_{mm',\mathbf{R}}^{(\text{H})} + V_{mm',\sigma,\mathbf{R}}^{(\text{xc})} \right. \\
&\quad \left. + V_{mm',\mathbf{R}}^{(\text{ext})} \right] D_{mm',\sigma,\mathbf{R}} \\
&\equiv \sum_{mm',\sigma,\mathbf{R}} \mathcal{K}_{mm',\sigma,\mathbf{R}} D_{mm',\sigma,\mathbf{R}}, \quad (49)
\end{aligned}$$

where  $V_{mm',\mathbf{R}}^{(\text{H})}$  and  $V_{mm',\sigma,\mathbf{R}}^{(\text{xc})}$  are the matrix elements of  $v_{\text{H}}$  and  $v_{\text{xc}}$  between the basis orbitals. For every fixed value of  $n_{m\sigma}^{(0)}$ , we can optimize  $\mathcal{F}$  with respect to the two densities  $n^{(0)}(\mathbf{r})$  and  $n(\mathbf{r})$ . In practice, by inspection of equations (35), (36) and (37) one can see that this is equivalent to a minimization with respect to the Slater determinant  $|\Psi_0\rangle$  and the Gutzwiller parameters contained in the operator  $\hat{\Phi}$ . This minimization can be carried out in two separate steps:

1. first carry out a Siesta self-consistent calculation to find the Slater determinant  $\Psi_0$  that optimizes  $\mathcal{F}[n(\mathbf{r}), n^{(0)}(\mathbf{r}), n_{m\sigma}^{(0)}]$  with respect to  $n^{(0)}(\mathbf{r})$ , enforcing the constraint (45) through an Augmented Lagrangian Method<sup>46</sup>. The Gutzwiller parameters, and therefore the hopping renormalization parameters  $R_{m\sigma}$ , are kept fixed throughout this

optimization. The atomic energy  $E_{\text{at}}[n(\mathbf{r})]$  does not change, nor does the double-counting energy  $E_{\text{dc}}[n^{(0)}(\mathbf{r})]$ , which is a function of  $n^{(0)}(\mathbf{r})$  only through  $n_{m\sigma}^{(0)}$ . The self-consistent single-particle Kohn-Sham equations allowing the minimization with respect to  $|\Psi_0\rangle$  are

$$\sum_{m'\mathbf{R}} \mathcal{H}_{mm',\sigma,\mathbf{R}} \psi_{m'\sigma,\mathbf{R}} = \varepsilon \psi_{m,\sigma,\mathbf{0}}, \quad (50)$$

where

$$\mathcal{H}_{mm',\sigma,\mathbf{R}} = \mathcal{K}_{mm',\sigma,\mathbf{R}} + V_{mm',\sigma,\mathbf{R}}^{(0)} - \lambda'_{mm',\sigma} \delta_{\mathbf{R}\mathbf{0}},$$

and

$$\begin{aligned}
V_{mm',\sigma,\mathbf{R}}^{(0)} &= \int d\mathbf{r} \phi_{m,\mathbf{R}}^*(\mathbf{r}) \left\{ v_{\text{H}}[n^{(0)}(\mathbf{r})] \right. \\
&\quad \left. + v_{\text{xc}}[n^{(0)}(\mathbf{r})] \right\} \phi_{m',\mathbf{0}}(\mathbf{r}). \quad (51)
\end{aligned}$$

2. next, optimize  $\mathcal{F}$  with respect to Gutzwiller parameters by a Lanczos-improved Levenberg-Marquardt (LM) algorithm (see Appendix C), enforcing the constraints (46) and (47). During this optimization, only the term  $\mathcal{K}[n(\mathbf{r})]$  and the atomic energy  $E_{\text{at}}[n(\mathbf{r})]$  in Eq. (48) are modified. These two quantities, together with the terms enforcing constraints for Gutzwiller parameters, build a quartic functional  $F_{\hat{\Phi}}$  of the matrices  $\hat{\Phi}$ , with explicit form

$$\begin{aligned}
F_{\hat{\Phi}} &= \sum_{m,m',\sigma} \left[ \mathcal{K}_{mm',\sigma,\mathbf{R}=0} \text{Tr} \left\{ \hat{\Phi}^\dagger \hat{n}_{mm',\sigma} \hat{\Phi} \right\} + R_{m\sigma}^\dagger \tau_{mm',\sigma} R_{m'\sigma} + \text{Tr} \left\{ \hat{\Phi}^\dagger \hat{H}_{\text{at}} \hat{\Phi} \right\} \right. \\
&\quad \left. - \lambda_{mm',\sigma} \left( \text{Tr} \left\{ \hat{\Phi}^\dagger \hat{\Phi} \hat{n}_{mm',\sigma} \right\} - n_{m\sigma}^{(0)} \delta_{mm'} \right) - \lambda_0 \left( \text{Tr} \left\{ \hat{\Phi}^\dagger \hat{\Phi} \right\} - 1 \right) \right], \quad (52)
\end{aligned}$$

where  $\tau_{mm',\sigma}$  is

$$\tau_{mm',\sigma} = \sum_{\mathbf{R} \neq 0, mm'} \mathcal{K}_{mm',\sigma,\mathbf{R}} D_{mm',\sigma,\mathbf{R}}^{(0)}. \quad (53)$$

These two steps are repeated one after the other until

self-consistency is achieved over both densities  $n(\mathbf{r})$  and  $n^{(0)}(\mathbf{r})$ . Once converged, we are left with a total energy functional depending on the diagonal matrix elements  $n_{m\sigma}^{(0)}$ , and that can be optimized by steepest descent, so

as to fulfill the stationary equations

$$\frac{\partial \mathcal{K}[n(\mathbf{r})]}{\partial n_{m\sigma}^{(0)}} - \frac{\partial E_{\text{dc}}[n^{(0)}(\mathbf{r})]}{\partial n_{m\sigma}^{(0)}} + \lambda_{mm,\sigma} + \lambda'_{mm,\sigma} = 0. \quad (54)$$

The terms appearing in the above equations are the only ones depending on the local uncorrelated density matrix  $n_{m\sigma}^{(0)}$ . The double-counting energy is a function of this density matrix only, while the functional  $\mathcal{K}$ , containing the renormalized density matrix  $D_{mm',\sigma,\mathbf{R}}$ , depends on  $n_{m\sigma}^{(0)}$  through the wavefunction renormalization parameters  $R_{m\sigma}$ .

### B. Atomic basis set angular momentum dependent renormalization for transition metals

Equations (33) and (34) describe a density matrix on a basis of orthogonalized atomic orbitals. For a system described by a single set of atomic  $d$ -orbitals, the indices  $m$  and  $m'$  are allowed to run on every value of the magnetic quantum number,  $m = \{-2, -1, 0, 1, 2\}$ . For a cubic system, the basis which diagonalizes the one-body density matrix  $D_{\mathbf{R},mm'}$  for  $\mathbf{R} = 0$  is the basis of  $d$  orbitals which have real harmonics as their angular part, so that  $m = \{r^2 - 3z^2, x^2 - y^2, xy, xz, yz\}$ , or in the language of group representations,  $m = \{e_g^{(1)}, e_g^{(2)}, t_{2g}^{(1)}, t_{2g}^{(2)}, t_{2g}^{(3)}\}$ . In general, simulating the electronic structure of a transition metal with an atomic basis set, such as the Siesta code does, will require also  $s$  orbitals to be present in the set, as well as  $p$  orbitals in order to allow for polarization of  $d$  and  $s$  atomic orbitals due to the cubic crystal field. We need therefore to reframe Eq. (37) by adding an additional couple of indices  $l = 0, 1$  besides  $l = 2$ . Since we assume for simplicity that Gutzwiller renormalization affects only  $d$ -type orbitals, we have that

$$D_{lm'l'm',\sigma,\mathbf{R}} = R_{m\sigma}^{l\dagger} D_{lm'l'm',\sigma,\mathbf{R}}^{(0)} R_{m'\sigma}^l, \quad (55)$$

with

$$R_{m\sigma}^l = \begin{cases} R_{m\sigma}; & l = 2 \\ 1; & l = 1, 0 \end{cases}, \quad (56)$$

for the  $\mathbf{R} \neq 0$  part, and

$$D_{lm'l'm',\sigma,\mathbf{R}=0} = \begin{cases} D_{lm'l'm',\sigma,\mathbf{R}=0}^{(0)}; & l \neq 2, l' \neq 2 \\ \delta_{ll'} n_{m\sigma} & l = 2, \end{cases} \quad (57)$$

with  $n_{m\sigma} = \text{Tr} \left\{ \hat{\Phi}^\dagger \hat{n}_{mm',\sigma} \Phi \right\}$ , for the on-site  $\mathbf{R} = 0$  part. In what follows the matrices  $D$  and  $n$  without angular momentum indices will refer to the density matrices of the subset of orbitals with  $l = 2$ . For any value of  $l$ , we will assume the indices  $m$  and  $m'$  to run on the cubic harmonics for that value of  $l$ , which ensures the  $\mathbf{R} = 0$  one-body density matrix to be diagonal, or, in other words, “natural”.

The Siesta code provides also the possibility to use a double set of  $d$ -type orbitals together with one set of  $s$  and one set of  $p$ . The use of two sets of  $d$ -orbital (double- $\zeta$  basis set), as opposed to a single set (single- $\zeta$ ) is particularly indicated for GGA calculations, in which small changes in the density profile of electrons lying close to the Fermi energy can affect the calculation of the energy much more than in LDA. While the first  $d$ -type basis set is more atomic like and more suited for an LDA+U or LDA+G calculation, the second  $d$ -type set has a larger spread, since it is meant to describe better also the tails of the density distribution. For LDA+G calculations we will therefore adopt a single- $\zeta$  basis set, while we will use a double- $\zeta$  basis set for all GGA calculations we perform and compare our LDA+G results with.

## III. RESULTS

### A. Nonmagnetic iron

In order to assess the effect of Gutzwiller renormalization parameters  $\Phi$  on the eigenvalues of the single-particle Kohn-Sham Hamiltonian at density self-consistency, we show in Fig. 1 the band structure of nonmagnetic iron for different values of interaction parameters  $U$  and  $J$  in the atomic Hamiltonian

$$\hat{H}_{\text{at}} = U/2 \hat{N}(\hat{N} - \hat{1}) - J|S^2| - \kappa|\hat{L}^2|, \quad (58)$$

where the parameter  $\kappa$  has been added in order to single out the effect of Hund’s third rule. The value of  $\kappa \approx 0.2$  eV can be estimated from spectroscopic data such as those of Corliss and Sugar<sup>47</sup>; a guess for a reasonable value of  $J = 1.2$  eV may be obtained either from spectroscopic data or from its expression in terms of Slater integrals  $F_2$  and  $F_4$ . Calculation of  $F_2$  and  $F_4$  has been done using the electronic structure program by Cowan<sup>48</sup>, and its results are in agreement with spectroscopic data. The band structures plotted in Fig. 1 are obtained by performing only the first and second optimization steps explained above, while the matrix  $n_{m\sigma}^{(0)}$  is kept fixed to its LDA value. In section Sect. III B we will show that even when  $n_{m\sigma}^{(0)}$  is treated as a variational parameter, its change with respect to the LDA value is very small in the case of nonmagnetic iron. An immediate consequence of the fact that we fix  $n_{m\sigma}^{(0)}$  is that we do not need to worry about the explicit form of the double-counting energy  $E_{\text{dc}}$  for the Hamiltonian (58), which plays a role in determining the electronic structure only through the optimization of the natural density matrix. In Table I we show the band mass renormalization factors  $Z_{e_g}$  and  $Z_{t_{2g}}$  for different values of Hubbard parameter  $U$ , whereas  $J$  is kept fixed along all rows of the table but the last one, where it is increased to 2.2 eV. Our method, as expected, appears unable to reproduce the orbital selective Mott transition of the  $e_g$  orbitals, obtained by Anisimov and coworkers<sup>27</sup> as a result of a DMFT calculation. In fact,

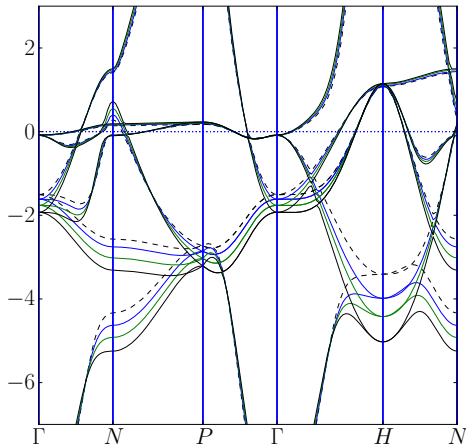


Figure 1. (Color online) Band structure results for a Siesta LDA+G calculation of nonmagnetic *bcc* iron without optimization of the natural density matrix  $n_{m\sigma}^{(0)}$ . The atomic interaction Hamiltonian we used is displayed in Eq. (58), and the values for its parameters are listed in Table I. The black solid line corresponds to  $U = 0$  and  $J = 0$ , the green line to  $U = 5$ ,  $J = 1.2$ , the blue line to  $U = 10$ ,  $J = 1.2$ , the dashed line to  $U = 10$  and  $J = 2.2$ . Values of  $U$ ,  $J$  and  $y$ -axis energies are in eV. The labels indicating the high-symmetry points for the  $k$ -point path are taken from reference<sup>49</sup> for the body-centered cubic lattice.

we find only a minor localization of both  $e_g$  and  $t_{2g}$  orbitals, driven both by the Hubbard interaction  $U$  and by Hund's exchange  $J$ . The latter plays a major role in the orbital-selectivity of the mass enhancement, as can be seen from the last row of Table I. It is at this stage not possible to clarify how much the weaker orbital selectivity resulting from our calculation could be due to the limitations of the Gutzwiller method or perhaps by the fact that our calculation is performed at zero temperature, as opposed to the finite temperature approach by Anisimov and coworkers.

### 1. Impact of hybridization between atomic orbitals on the description of a Mott phase

The minor correlation-induced enhancement of  $e_g$  band mass with respect to the LDA results may be connected to the sizable hybridization connecting  $e_g$  orbitals on a site to  $s$ -orbitals on neighboring sites. This hybridization is ineffective close to the  $\Gamma$  point, where the  $e_g$  band remains quite flat, but is able to induce an appreciable dispersion in the rest of the Brillouin zone, especially close to the  $H$  point. The local Gutzwiller projector that we use can only provide a  $\mathbf{k}$ -independent renormalization  $Z$ , and is thus unable to distinguish between the flat dispersion near the  $\Gamma$  point, and e.g., the wider one around the  $H$  point. In other words  $Z$  should be regarded as an

$U$ (eV)	$\langle(\Delta N)^2\rangle$	$ S $	$ L $	$Z_{e_g}$	$Z_{t_{2g}}$
0	2.30	0.89	3.22	1.	1.
2.5	1.37	1.00	3.27	0.94	0.96
5	1.10	1.03	3.29	0.90	0.93
10	0.82	1.04	3.31	0.82	0.87
10*	0.78	1.25	3.05	0.72	0.82

Table I. Variance of  $d$ -electron number operator, total spin and angular momentum for  $d$  orbitals, band mass renormalization factors for  $e_g$  and  $t_{2g}$  orbitals for a LDA+G calculation without optimization of the natural density matrix, for the atomic Hamiltonian displayed in Eq. (58). The value of  $\kappa$  is 0.2 eV and the value of  $J$  we used was always 1.2 eV, except for the row marked with a dot ( $\cdot$ ), for which  $J = 0$ , and the row marked with an asterisk ( $*$ ), for which  $J = 2.2$ . The values of  $U$  we used are listed in the first column. The band structure results corresponding to the first and to the last three rows of the table are plotted in Fig. 1. The last line of the table shows how orbital selectivity is more sensitive to Hund's exchange  $J$  than to Hubbard  $U$ .

average of the quasi-particle weight over the whole Brillouin zone, indeed a major limitation of the GA. In the specific example of *bcc* iron, it is just the hybridization with the weakly correlated  $s$ -orbitals that prevents a genuine Mott localization of  $e_g$  orbitals within the Gutzwiller approximation. In fact, the condition for a Mott transition to occur within the Gutzwiller approximation is that the band-energy gain  $E_{\text{kin}}$  upon delocalizing quasiparticles does not compensate anymore the cost in Hubbard repulsion  $E_{\text{Hub}}$ . In the single-band Hubbard model it can be shown that the Hubbard repulsion

$$E_{\text{Hub}} = \frac{U}{4} (1 - \sqrt{1 - R^2}),$$

while  $E_{\text{kin}} = R^2 E_{\text{kin}}^{(0)}$ , where  $E_{\text{kin}}^{(0)} < 0$  is the non interacting value. As a result, for  $U \geq -8E_{\text{kin}}^{(0)}$  the hopping energy gain cannot compensate anymore the Hubbard repulsion and the lowest energy solution is characterized by  $R = 0$ , which describes the Mott insulator. When however, as in the present multi-band case, the main part of the band energy is renormalized by a *single*  $R$ , we have that  $E_{\text{kin}} \propto -R$  while still  $E_{\text{Hub}} \propto R^2$  for  $R \ll 1$ , so that there is always a minimum with  $R$  finite, which is what we do find.

However, in spite of the fact that correlation effects seem not to play a major role in the band structure, they substantially affect the magnetic properties, as we are going to show in what follows.

### B. Ferromagnetic and paramagnetic iron: correlation-induced enhancement of local magnetic moment

In order to study magnetic properties of iron, we performed unpolarized and polarized LDA, GGA and LDA+G calculations, including in the latter also the optimization with respect to the natural density-matrix. In

	$n_\alpha^{(0)}$	$m/m^*$
LDA unp.	0.597,0.685	1.,1.
LDA pol.	0.920,0.823,0.303,0.515	1.,1.,1.,1.
LDA+G unp.	0.599,0.673	0.925,0.953
LDA+G pol.	0.936,0.880,0.277,0.457	0.969,0.967,0.984,0.984

Table II. Orbital densities  $n_\alpha^{(0)}$  and quasi-particle mass renormalization  $m/m^* = R_{\alpha\alpha}^2$  for the different types of simulations performed, with  $\alpha = e_g, t_{2g}$  and  $e_g \uparrow, t_{2g} \uparrow, e_g \downarrow, t_{2g} \downarrow$  for unpolarized (unp.) and polarized (pol.) calculations respectively.

	$a_{\text{lat}}$ (Å)	$m$	$m_d$	$2 S $
GGA unp.	2.80	—	—	—
GGA pol.	2.87	2.33	—	—
LDA unp.	2.77	—	—	1.77
LDA pol.	2.83	2.066	2.14	2.61
LDA+G unp.	2.86	—	—	2.47
LDA+G pol.	2.87	2.44	2.58	3.04
Exp.	2.87	2.22	—	—

Table III. Results for optimized lattice parameter  $a_{\text{lat}}$  (in Å), total magnetization  $m$ , magnetization  $m_d$  on  $d$ -type orbitals, and total spin  $2|S|$  (in Bohr magnetons) on  $d$  orbitals. The last row shows the experimental values for lattice parameter and magnetization.

Tables II to VI we list the electronic structure data of *bcc* iron with optimized  $n_{m\sigma}^{(0)}$ . The adopted values of  $U$  and  $J$ , see Eqs. (11) and (13), are 2.5 eV and 1.2 eV respectively, both slightly larger than those used by Anisimov and coworkers<sup>27</sup>. We observe, see second column of Table II, that the optimization of  $n_{m\sigma}^{(0)}$  in the LDA+G unpolarized case causes only small changes in the matrix elements of the natural density matrix with respect to the LDA result. This is an *a posteriori* justification of the results obtained in Sect. III A, and suggests that such a value is mainly determined by electrostatic balance, which is well captured by LDA and does not require a better account of correlation effects. The Gutzwiller parameters do provide the wavefunction with more flexibility, but do not seem to give any important feedback on the natural density matrix.

This feedback becomes instead important in the spin polarized case, where it contributes to an increase in total magnetization  $m$  as well as of the lattice parameter, as can be seen by comparing the values in the second column of Table III.

Within our Gutzwiller approach we are also able to compute the local spin moment  $|S|$  on  $d$ -type orbitals, from the expectation value of  $S^2$

$$S(S+1) = \text{Tr} \left\{ \hat{\Phi}^\dagger S^2 \hat{\Phi} \right\}. \quad (59)$$

This magnetic moment is partially aligned to the  $z$  axis, thus contributing to the total magnetization  $m$ , which is instead computed from the Gutzwiller-renormalized den-

sity  $n(\mathbf{r})$  as

$$m = \int d\mathbf{r} [n_\uparrow(\mathbf{r}) - n_\downarrow(\mathbf{r})]. \quad (60)$$

It is worth remarking that the increase of  $2|S|$  from LDA to LDA+G polarized calculations is almost equal to the simultaneous increase in magnetization, suggesting that the magnetization rise caused by LDA+G is mainly due to the larger local magnetic moment available due to correlations.

### C. Energy balance in ferromagnetic vs. paramagnetic iron

We observe that, when magnetism is allowed, the magnitude of the  $d$ -orbital local moment  $|S|$  increases less within LDA+G, roughly 20%, than LDA, around 50%. In other words, nonmagnetic, unpolarized LDA+G already provides iron with local moments of the right order of magnitude, ready to align together when given the possibility. The propensity towards magnetic order in LDA+G has its counterpart in the balance of the various contributions to the total energy. In Table IV we list the total energies of the various density functional calculations which we carried out, and in Table V the energy differences between polarized and unpolarized calculations. In both tables the total energy is divided up into kinetic, electron-ion interaction plus electrostatic, and exchange-correlation contributions. In Table VI we indicate the error of LDA+G arising from the linearization (42) and (43) of the Hartree and exchange-correlation energies, respectively. We observe that these errors are much smaller than the energy differences in Table V, which are therefore reliable estimates.

Focusing on the last two rows in Table V, we note a most interesting fact. While in LDA the onset of magnetism is accompanied by a loss of kinetic energy overwhelmed by a gain in electron-ion, Hartree and exchange potential energies, *the opposite* actually occurs in LDA+G. Upon addition of electron correlation effects through LDA+G, *bcc* iron emerges as a correlated material, where magnetism appears as the ordering of pre-existing moments driven by kinetic rather than potential energy gain. With the moderate and controlled improvement represented by Gutzwiller projection over LDA, the basic physical reason why the atomic magnetic moments of iron order ferromagnetically turns completely around, from the inter-site exchange upon which the itinerant Stoner picture is based, to one that is closer to double exchange. Ferromagnetism is necessary to allow the  $t_{2g}$  electrons (actually "holes") to propagate and thus reduce their kinetic energy,<sup>50,51</sup> as in the manganites.<sup>31</sup>

More in detail, the gain in kinetic energy is signaled by the fact that the quasi-particle weights  $Z$  increase when a finite magnetization is allowed to appear, as can be seen in Table II. This result, that quasiparticles propagate better in presence of ferromagnetic order, supports the

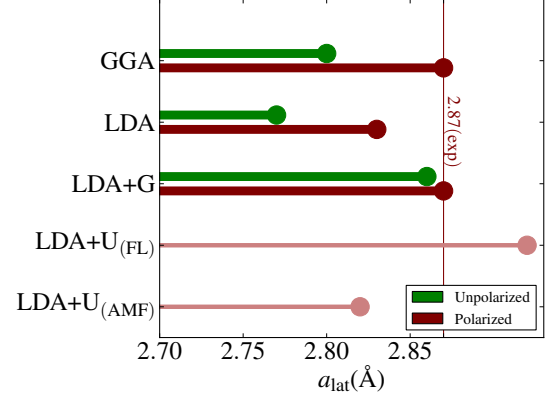
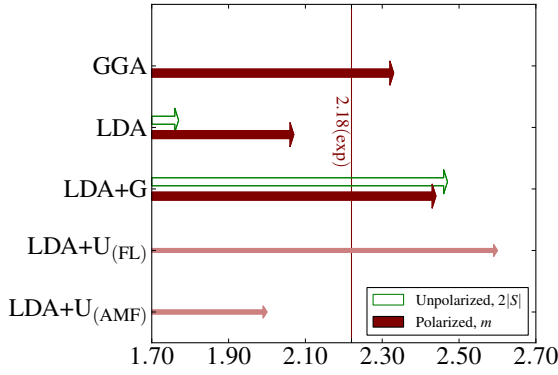


Figure 2.

Figure 3. (Color online) Top left: magnetic moment  $2|S|$  (for unpolarized calculations, empty green arrows) and magnetization  $m$  (for polarized calculations, filled dark red arrows) within GGA, LDA, LDA+G. The last two thin pink arrows refer to previous calculations by Cococcioni and De Gironcoli<sup>38</sup>. Top right: lattice parameters listed for the same calculations (green unpolarized, red polarized, pink from reference<sup>38</sup>). The figures plotted in these graphs are listed also in Table III.

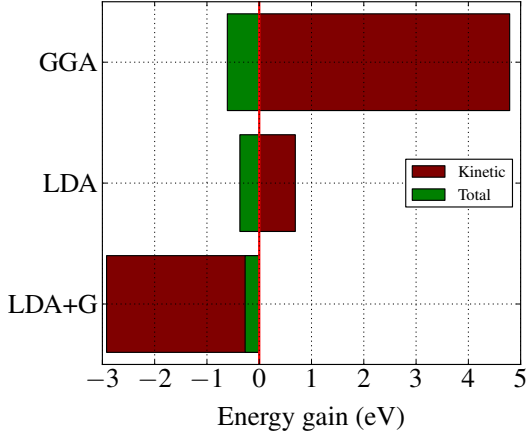


Figure 4. (Color online) Total (green) and kinetic (red) energy gain (in eV per atom) of the spin polarized relative to the spin unpolarized phase of *bcc* iron. The values plotted are listed along the second and third columns of Table VI.

view of a double-exchange mechanism, a suggestion that would be better evidenced if we could have a  $\mathbf{k}$ -resolved evaluation of quasiparticle weights. Double-exchange is an intrinsically many-body effect which cannot be reproduced within theories that do not include bandwidth, or kinetic energy renormalization due to electron-electron interaction. For this reason it was not uncovered by previous DFT calculations, whereas it would naturally occur as a consequence of Anisimov's selective  $e_g$  Mott localization. The double-exchange process can only set in in presence of long-lived on-site magnetic moments, independently of their inter-site order-

	$E_{\text{tot}}$	$E_{\text{kin}}$	$E_{\text{at+el}}$	$E_{\text{xc}}$
GGA unp.	-781.625	765.108	-1157.611	-389.121
GGA pol.	-782.235	769.901	-1161.603	-390.533
LDA unp.	-780.196	777.255	-1170.507	-386.943
LDA pol.	-780.567	777.947	-1171.205	-387.308
LDA+G unp.	-777.231	777.099	-1168.651	-385.682
LDA+G pol.	-777.499	774.182	-1165.568	-386.117

Table IV. Total energy (eV/atom) for *bcc* iron computed with the different basis sets and functionals, divided in total energy, kinetic energy, atomic interaction plus electrostatic energy  $E_{\text{at+el}}$ , and exchange-correlation energy. The quantity on the fourth column is equal to  $E_{\text{at+el}} = E_{\text{ion}} + E_{\text{ie}} + E_{\text{H}} + E_{\text{at}} - E_{\text{dc}}$ , where  $E_{\text{at}}$  is defined in Eq. (41),  $E_{\text{dc}}$  is defined in Eq. (13), and  $E_{\text{ie}}$  and  $E_{\text{ion}}$  are the electrostatic interaction energies between ions and electrons and between ions and ions. The

ing. An independent-electron, single-Slater-determinant theory as HF, or LDA can only describe the birth of a magnetic moment through the simultaneous appearance of a net spin polarization. This same magnetization, hence the presence of a majority spin component, is able to decrease electron-electron interaction energy through the Pauli exclusion principle and to increase electron localization because of phase-space shrinking. The latter has as a natural effect also the increase of kinetic energy, a characteristic result of the so-called Stoner-Wohlfarth picture<sup>52</sup> that we now find in disagreement with our results for iron.

The results outlined above, although in qualitative agreement with the views of Anisimov *et al.*, are sufficiently strong to call for an independent assessment for the accuracy of the Gutzwiller approach. A comforting check is provided by comparison of the band structures

	$\delta E_{\text{tot}}$	$\delta E_{\text{kin}}$	$\delta E_{\text{at+el}}$	$\delta E_{\text{xc}}$
GGA	-0.61	4.79	-3.992	-1.412
LDA	-0.37	0.692	-0.698	-0.365
LDA+G	-0.27	-2.92	3.083	-0.44

Table V. Energy differences (eV/atom) between the spin-polarized and unpolarized ground-states of *bcc* Fe, taken from Table IV. By looking at the last two columns, one notices the opposite signs of kinetic and  $E_{\text{at+el}}$  gains when switching between the two ground-states. The kinetic energy gain is connected with the increase of Gutzwiller band mass renormalization factors  $Z$  from spin unpolarized to spin polarized wavefunctions, as can be seen from Table II.

	$\Delta E_{\text{H}}$	$\Delta E_{\text{xc}}$
LDA+G unp.	0.0083	-0.0012
LDA+G pol.	0.0054	-0.0020

Table VI. Estimated errors (in eV) due to the approximate expressions (42) and (43) for the Hartree and exchange-correlation energies respectively, listed for the spin unpolarized and spin polarized ground-state calculations. All errors are negligible with respect to the energy differences computed in Table V.

and density of states obtained within LDA, LDA+G and GGA, shown from Fig. 5 to Fig. 8, and from Fig. 3, showing the estimated lattice parameters, magnetization and total magnetic moments within the same three functional schemes. The spin-polarized GGA is generally considered as a reliable approach to transition metals, as is able to provide a very good estimation of their lattice constants and magnetic moments. The Siesta GGA prediction for the iron lattice parameter is 2.87 Å, in good agreement with the experimental value, while its magnetic moment is slightly overestimated (2.33 vs. 2.22 Bohr magnetons, see ). We note that LDA+G corrects, without a need for gradient terms, the lattice parameter underestimation which is a well known flaw of LDA. LDA+G also increases the total magnetic moment from the underestimated LDA value to a slightly overestimated one, now larger than the GGA result (see again Fig. 3). Comparing the polarized band structures, we note an upward shift of the minority band in LDA+G with respect to GGA, consistent with the larger magnetization obtained by the former, although the shapes are quite similar. In particular, the minority band at  $\Gamma$  within LDA+G lies above the Fermi energy, while it is below in GGA, and in experiments.<sup>53</sup> The detailed band behavior near  $\Gamma$  is notoriously delicate, as recently discussed by Ref. 54, and crucially depends on all parameters that contribute to determine the precise value of magnetization, not least the uncertainty in the expression of the double-counting term. Previous LDA+U calculations on iron<sup>37,38</sup> indeed pointed out the differences arising by using an around-mean-field instead of a fully-localized expression for the double-counting energy, a question that would be worth

of further investigation.<sup>55</sup>

#### IV. FINAL REMARKS

We presented here an explicit and careful implementation of a self-consistent scheme integrating the standard local density functional formalism of Kohn and Sham DFT with that implied by Gutzwiller wavefunction correctionsGA.

Other applications of the Gutzwiller method to realistic electronic structure calculations have recently appeared. Bünemann, Weber and Gebhardt<sup>56–58</sup> implemented a non self-consistent Gutzwiller approach to electronic structure calculations, where a tight-binding model was set up from effective hopping parameters computed through a Kohn-Sham density functional calculation, and afterwards solved within the multi-band GA. An approach where both density and Gutzwiller parameters are optimized self-consistently was proposed in Refs. 19 and 20, and applied to several case studies.<sup>22,24</sup> This method is in principle similar to ours, with the difference that it does not include the possibility of using a projector with nonzero off-diagonal matrix elements, which is instead a natural feature of our mixed-basis parametrization with  $\hat{\Phi}$  operators. More recently, a fully unrestricted and density self-consistent Gutzwiller+LDA approach has been proposed<sup>23</sup> and applied to the  $\gamma$ - $\alpha$  iso-structural transition of Ce.<sup>25</sup> This method is in its formulation equivalent to ours, though the implementation is different.

As an important and basic application, we applied the resulting LDA+G method to the calculation of the electronic structure of *bcc* Fe, where important open questions about the role of correlations still remain, including the possibility of an orbital-selective localization of  $e_g$  electrons, see Ref. 27 and references therein. Although we did not find an actual orbitally selective localization of electrons, our results confirm that the magnetism of iron is, at least partially, driven by a double-exchange mechanism, caused by stronger localization of  $e_g$  states relative to  $t_{2g}$  ones, a typically many-body phenomenon not described by conventional DFT. The double exchange mechanism would also arise as a direct consequence of a selective  $e_g$  Mott localization.

The Gutzwiller approach enables to compute local magnetic moments, including their enhancement due to interactions, already at the unpolarized LDA level. The spin-polarized calculation separately provides the energy gain caused by interatomic magnetic alignment and ordering. The two phenomena, onset of magnetic moment and ordering, which come by necessity together and are treated on the same footing within simple LDA, Local Spin Density Approximation (LSDA) and LDA+U, are correctly very distinct within LDA+G. The present calculations of the electronic structure of Fe through LDA+G implemented in the Siesta code could be further perfected. For example, and first of all, with the

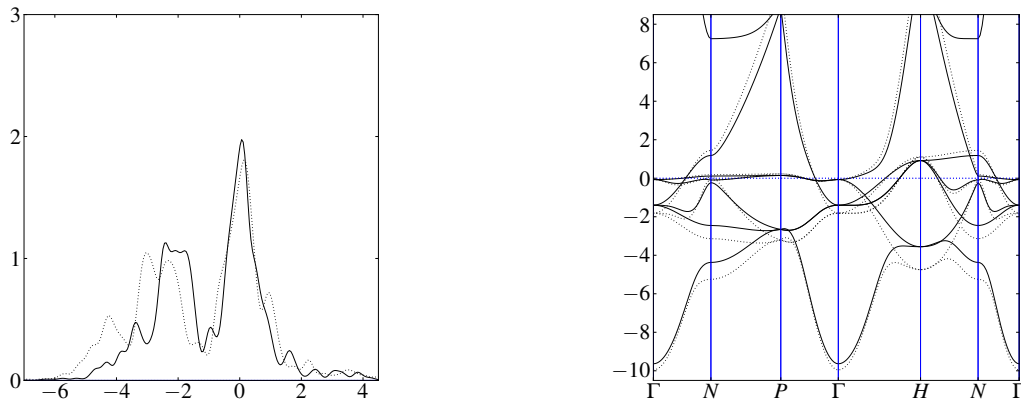


Figure 5. (Color online) Comparison of projected density of states and band structure between spin unpolarized LDA+G (solid lines) and LDA (dotted lines).

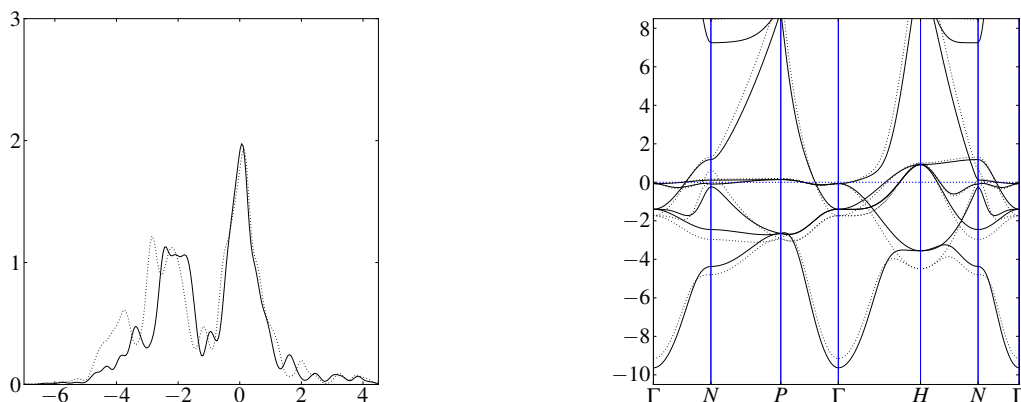


Figure 6. (Color online) Comparison of projected density of states and band structure between spin unpolarized LDA+G (solid lines) and GGA (dotted lines).

inclusion of two separate hopping renormalization factors on each  $e_g$  and  $t_{2g}$  multiplet of a double- $\zeta$  basis set, through which we will be able to better account for the effects of Hubbard- $U$  and exchange parameter  $J$  on electron localization. The slightly excessive magnetic moment found can most likely be corrected through a better choice for the Hubbard- $U$  and by an improved evaluation of double-counting energy. In spite of the great number of parameters contained in  $\hat{\Phi}$ , the Lanczos-enhanced LM algorithm we implemented here for the minimization of the energy with respect to Gutzwiller parameters is stable and fast, and can be easily parallelized to deal with more complex system as crystals having more than one atom per unit cell as transition metal compounds.

## V. ACKNOWLEDGMENTS

We thank Nicola Lanatà for useful suggestions and discussions. This project was completed during the tenure in Trieste of contracts PRIN/COFIN 2010LLKJBX 004, EU-Japan Project LEMSUPER, grant agreement 283214, Sinergia CRSII2136287/1 and ERC Advanced Grant 320796 MODPHYSFRICT. We also acknowledge financial support by the European Union, Seventh Framework Programme, under the project GO FAST, grant agreement no. 280555.

### Appendix A: Imposing symmetries on the Gutzwiller projector

The easiest basis in which to define the Gutzwiller projector is the basis of Slater determinants of single-

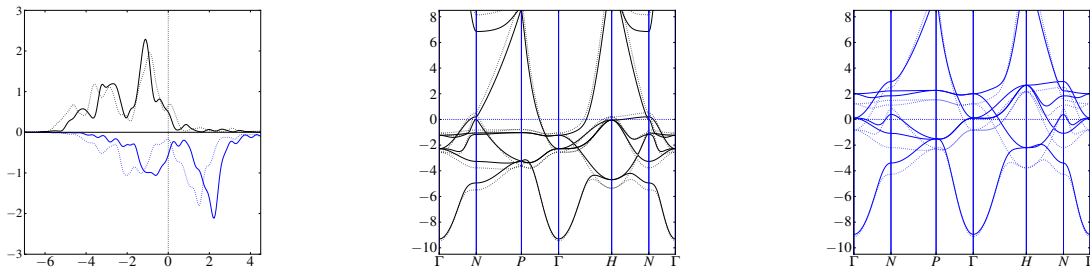


Figure 7. (Color online) Comparison of projected density of states and band structure between spin polarized LDA+G (solid lines) and LDA (dotted lines). The line colors blue and black refer to minority and majority component respectively.

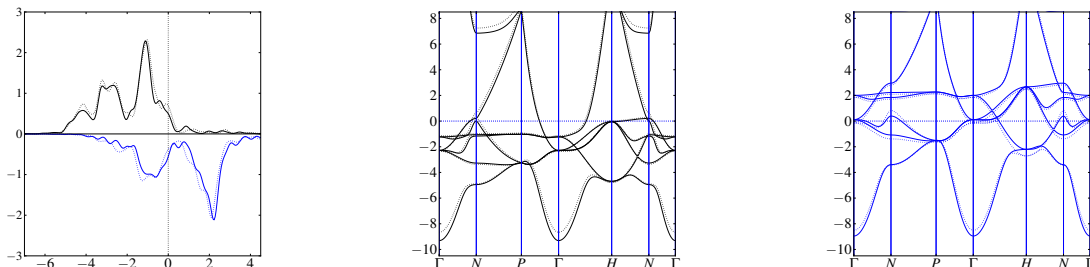


Figure 8. (Color online) Comparison of projected density of states and band structure between spin polarized LDA+G (solid lines) and GGA (dotted lines). The line colors blue and black refer to minority and majority component respectively.

particle wavefunctions, that we indicate in the text as basis of electronic configurations (BC). A sample  $N$ -particle configuration on  $d$  orbitals is for instance the 5-electron, maximum-spin configuration, which in second quantized form reads

$$\left( \prod_{m=-2}^2 \hat{c}_{m\uparrow}^\dagger \right) |0\rangle. \quad (\text{A1})$$

If we wish to write the most general projector in the BC, the number of parameters we need is in principle equal to  $2^{2(2l+1)} \times 2^{2(2l+1)}$ , where  $2^{2(2l+1)}$  is the size of the many-body Hilbert space for multiplet of orbitals of angular momentum  $l$ . This is a huge number, which is hardly possible to treat in with numerical optimization already when  $l = 4$  or  $5$ . In order to lower the amount of parameters that build up a Gutzwiller projector, we need to switch from this type of configuration basis, whose states are identified by single-particle quantum numbers as single particle spin  $\sigma$ , and magnetic quantum number  $m$ , to a basis of multi-particle quantum numbers that are good quantum numbers of the problem we are studying, which are, in the case of a system with full rotational invariance, the total spin  $S^2$ , the total angular momentum  $L^2$ , and the total spin and angular momentum magnetic quantum numbers  $S_z$  and  $L_z$ . We will refer to this basis of many-body states labeled by good quantum numbers of the problem as to the many-body symmetric basis (MBSB).

In the case of paramagnetic iron, the orbital rotational symmetry is broken by the cubic crystal field, resulting in a different set of conserved orbital quantum numbers, corresponding to the irreducible representations of the cubic group. In the case of spin-polarized iron, also the spin rotational invariance is broken in favor of a lower spin easy-axis symmetry, where only  $S_z$  remains a good quantum number.

### 1. Spin rotational symmetry

It is well-known (see for instance Ref. 59) that the eigenstates of the total spin operator square  $S^2$  on the basis of a set of  $N$  spins can be written in terms of Young tableaux. This is possible because of the isomorphism between the group  $SU(N)$  and the irreducible representations of the permutation group, which are represented by Young tableaux. A general tableau provides a rule for the symmetrization-antisymmetrization with respect to particle exchange of a Slater determinant with a given number of electrons in a given orbital and spin configuration. Each box of a tableau corresponds to a particular filled single-particle orbital state, containing either a spin up ( $\uparrow$ ) or a spin down ( $\downarrow$ ) electron. The orbitals belonging to the same row of a tableau must be symmetrized, while those belonging to different rows must be antisymmetrized. The many-body wavefunction pro-

duced by this symmetrization-antisymmetrization recipe turns out to be an eigenstate of both  $\hat{S}^2$  and  $\hat{S}_z$ . The eigenvalue of  $\hat{S}_z$  can be obtained by summing the spins in each box of the tableau, while the eigenvalue of  $\hat{S}^2$  corresponds to the tableau shape. For instance, the state with maximum  $S_z$  component on  $d$  orbitals is built from the totally symmetric tableau

$$\boxed{\uparrow \uparrow \uparrow \uparrow \uparrow}, \quad (\text{A2})$$

which corresponds to  $S = 5/2$ . This particular state is a single Slater determinant, already belonging to basis of configurations. The row-wise antisymmetrization rule of a tableau automatically imposes Pauli principle on the wavefunction, so that only wavefunctions obtained from one-column tableaux, or two-column tableaux with opposite spins on each column, are non-zero. For instance, the two-particle singlet state has a simple representation in terms of the totally antisymmetric two-particle tableau

$$\boxed{\begin{array}{c} \uparrow \\ \downarrow \end{array}}, \quad (\text{A3})$$

applied to a couple of electrons with opposite spin. By application of raising and lowering operators  $\hat{S}_+$  and  $\hat{S}_-$  on a many-body wavefunction, one obtains another wavefunction which is generated by a tableau of the same shape. Every wavefunction with fixed values of  $S$  and  $S_z$  has an additional degeneracy which can be computed from the shape of the generating tableau, according to some simple rules<sup>59</sup>.

## 2. Implementation of crystal point symmetry

In order to provide a classification of many-body wavefunctions according to point group quantum numbers, it is necessary to label them with angular momentum quantum numbers.

### a. Building eigenstates of angular momentum

Thanks to Young tableaux we are able to label states with the quantum numbers  $\{N, S^2, S_z, L_z\}$ . For each of these sets of quantum numbers, there are several states with different values of the square modulus  $L(L+1)$  of total angular momentum. If the BC of our problem is already built from single-particle eigenstates of  $\hat{L}_z$  and  $\hat{L}^2$ , as for instance the  $3d$  orbitals of a transition metal ( $l = 2$ ), it is very easy to build the angular momentum raising operator explicitly

$$\hat{L}_+ = \sum_{m=-l}^{l-1} \sqrt{l(l+1) - m(m+1)} \hat{c}_{m+1}^\dagger \hat{c}_m. \quad (\text{A4})$$

From  $\hat{L}^2 = \hat{L}_+ \hat{L}_- + \hat{L}_z (\hat{L}_z - 1)$  we can build the operator  $\hat{L}^2$ , which will be block-diagonal in every subspace with

fixed  $\{N, S^2, S_z, L_z\}$ . The diagonalization of every block gives the desired set of states, labeled by  $\{N, S^2, S_z, L_z\}$ . For large many-body spaces, as for instance the one built from  $d$ -electrons of a transition metal, another index  $\theta$  might be needed, in order to distinguish between different states having the same set of quantum numbers listed above.

## 3. Building eigenstates of point group symmetry operators

Provided that a set of many-body eigenstates of spin and angular momentum operators has been given, it is easy to break the rotational symmetry of the MBSB in favor of some lower crystal symmetry when necessary. In this section we will treat the case of cubic symmetry, which is the case of iron. The ingredients we need for this purpose are just the following:

1. the  $3 \times 3$  matrix representation  $G(g)_{ij}$  of the action of each element  $g$  of the cubic group on a three-dimensional vector  $\mathbf{r}$ ,
2. the character table of the group, for the cubic group it is shown in Table VII,
3. the  $\mathbf{r}$ -space representation in spherical coordinates of an external potential with the symmetry of the group; an example for a potential with cubic symmetry is

$$v[\hat{\mathbf{r}}(\theta, \phi)] = \cos(\theta)^4 + \frac{1}{4}[3 + \cos(4\phi)] \sin(\theta)^4, \quad (\text{A5})$$

where  $\hat{\mathbf{r}}$  is the radial unit vector.

	$E$	$8C_3$	$3C_2(C_4^2)$	$6C_2$	$6C_4$
$A_1$	1	1	1	1	1
$A_2$	1	1	1	-1	-1
$E$	2	-1	2	0	0
$T_1$	3	0	-1	-1	1
$T_2$	3	0	-1	1	-1

Table VII. (Color online) Character table of the cubic group. The first row lists all the group classes along with the number of symmetry operations they contain. The following rows list the irreducible representations, and their character on each symmetry class. From reference<sup>60</sup>.

Once these three ingredients are at hand, we proceed as follows:

- for each set of spherical harmonics  $Y_{L,m}(\theta, \phi)$  with given  $L$ , we compute (by means of the algorithm of Gimbutas *et al.*<sup>61</sup>) and diagonalize the matrix

$$C_{m,m'}^{(L)} = \int Y_{L,m}^*(\hat{\mathbf{r}}) v(\hat{\mathbf{r}}) Y_{L,m'}(\hat{\mathbf{r}}) d\Omega; \quad (\text{A6})$$

- for each set of spherical harmonics with given  $l$  and for each group element  $g$ , we calculate the matrix elements

$$M(g)_{m,m'}^L = \int Y_{L,m}^*(\hat{r}) Y_{L,m'}(G(g)^{-1}\hat{r}) d\Omega; \quad (\text{A7})$$

- for each eigenvalue  $\varepsilon$  of the matrix  $C^{(L)}$ , and for all eigenvectors  $c^{\varepsilon,L,i}$  relative to this eigenvalue, we compute the character

$$\chi(\mathcal{C}, L, \varepsilon) = \sum_i \sum_j c_j^{\varepsilon,L,i} M(g \in \mathcal{C})_{jk}^L c_k^{\varepsilon,L,i} \quad (\text{A8})$$

relative to the class  $\mathcal{C}$ . The value of the character enables us to assign the correct label of irreducible representation  $\mathcal{I}$  to the eigenvectors  $c^{\varepsilon,L,i}$ .

The matrices  $U_{ij}^{(L)} = c_j^{\varepsilon,L,i}$  are the unitary matrices we need to apply to every block of many-body basis states with a given value of  $L$  in order to switch from a basis labeled with  $\{N, S^2, S_z, L^2, L_z\}$  to a basis indicated by  $\{N, S^2, S_z, L^2, \mathcal{I}, \iota\}$ <sup>62</sup>, where  $\iota$  labels the states within the same irreducible representation  $\mathcal{I}$ .

## Appendix B: Building the most general Gutzwiller parameter matrix

In this section we show how to parametrize the matrix  $\hat{\Phi}$  of Gutzwiller parameters in the case of full spin and orbital rotational symmetry. The procedure is similar in the case of cubic symmetry.

We can easily construct the most general Gutzwiller parameter matrix  $\hat{\Phi}$  commuting with the operators  $S^2$ ,  $\hat{L}^2$ ,  $\hat{S}_{x,y,z}$  and  $\hat{L}_{x,y,z}$  by the following procedure. Operatively,

1. we find the quantum numbers that uniquely identify the irreducible representation of the symmetry group, in this case spin and spatial rotations  $SU(2) \times O(3)$ . These quantum numbers are  $\alpha = \{N, S, L\}$ . The same representation can appear multiple times, so we will add another quantum number  $\theta$  to distinguish between equivalent representations. Each irreducible representation has a degeneracy  $n_{\{\alpha,\theta\}} = L(L+1) \times S(S+1)$ ; we will distinguish between states that are a basis for the same irreducible representation  $\{\alpha, \theta\} = \{N, S, L, \theta\}$  through the index  $\iota = \iota(\alpha\theta)$ . In the case of spin and rotational symmetry  $\iota$  lists all the eigenstates of  $\hat{S}_z$  and  $\hat{L}_z$  within the same  $S$  and  $L$ .
2. With the previous definitions, the matrix elements of  $\hat{\Phi}$  are labeled

$$\Phi_{\alpha\theta\iota,\beta\theta'\iota'} = \delta_{\alpha\beta} \delta_{\iota\iota'} \phi_{\theta\theta'}^\alpha, \quad (\text{B1})$$

where  $\phi_{\theta\theta'}^\alpha$  is a reduced matrix element. The labels  $\alpha\theta\iota$  and  $\beta\theta'\iota'$  identify univocally one state of the MBSB, so that our parametrization of  $\hat{\Phi}$  is complete.

The same recipe holds when the spatial symmetry is, for example, the crystal cubic symmetry. In this case  $\alpha = \{N, S, \mathcal{I}\}$ .

The result expressed by Eq. (B1) comes directly from Schur's lemma, which states that a matrix commuting all the matrices of an irreducible representation of a group  $\mathcal{G}$  must be a multiple of identity. The matrix  $\Phi_{\alpha\theta\iota,\beta\theta'\iota'}$  must be nonzero only for  $\alpha = \beta$  since, if  $\hat{G}$  is a generator of the group and  $\varepsilon_\alpha$  its eigenvalue with respect to any basis vector belonging to irreducible representation  $\alpha$ , the commutation relations  $[\hat{\Phi}, \hat{G}] = 0$  imply that

$$\hat{G}\hat{\Phi}|\alpha\rangle = \hat{\Phi}\hat{G}|\alpha\rangle = \varepsilon_\alpha\hat{\Phi}|\alpha\rangle \quad (\text{B2})$$

and that  $\hat{\Phi}|\alpha\rangle$  must be a vector with the same quantum numbers  $\alpha$ .

Again from the condition of zero commutator, we have that  $\Phi_{\alpha\theta\iota,\alpha\theta'\iota'}$ , seen as a matrix in the indices  $\iota\iota'$  with fixed  $\theta = \theta'$ , must commute with all the matrices of irreducible representation  $\alpha$ , and by Schur's lemma it must be a multiple of the identity matrix. For  $\theta \neq \theta'$  the same statement does not hold, since the representations are distinct.

However, their equivalence implies that the matrices of the first are related to the matrices of the second through a unitary transformation. We can choose this transformation to be the identity, and this enables us to draw for  $\theta \neq \theta'$  the same conclusions as for  $\theta = \theta'$ , so that  $\Phi_{\alpha\theta\iota,\alpha\theta'\iota'}$  is diagonal in  $\iota\iota'$  irrespectively of  $\theta$  and  $\theta'$ .

### 1. Symmetry reduction of parameter space

The procedure explained in the previous paragraphs enables to considerably reduce the number of parameters for the Gutzwiller projector, so that its numerical optimization becomes not only computationally feasible, but also reasonably cheap. In Table VIII we list the sizes of local many-body irreducible representations and the number of independent Gutzwiller parameters compatible with a few different spin and point symmetries.

spin symmetry	point symmetry	# Hilbert	# $\Phi$
SU(2)	O(3)	81	121
U(1)	O(3)	176	336
SU(2)	cubic	197	873
U(1)	cubic	428	2716

Table VIII. Number of many-body irreducible representations generated by  $d$  electrons and size of Gutzwiller parameter space for different types of spin (first column) and point (second column) symmetries. The symbol U(1) refers to axial spin symmetry, SU(2) to full rotational symmetry, O(3) to full spatial rotational symmetry.

### Appendix C: Sparse-constrained Levenberg Marquardt algorithm

This algorithm performs the minimization of the Gutzwiller variational energy Eq. (52) with respect to the matrix elements of  $\hat{\Phi}$ . The details of the conventional constrained Levenberg-Marquardt (LM) algorithm are well explained by Fletcher<sup>46</sup>, who suggests the Multiplier Penalty Functional method (also known as Augmented Lagrangian method) as a way to impose constraints.

#### Levenberg-Marquardt algorithm with Lanczos approximation for the Hessian

Depending on the quantity of single-particle orbitals involved in the definition of the Gutzwiller parameter matrix, the number of parameters  $x_i$  in the block-diagonal matrix  $\Phi_{\alpha\beta}$  can be very large, which makes it computationally very expensive to compute the inverse Hessian matrix  $\mathbf{h}^{-1}$  which is needed in the LM algorithm in order to find the descent direction  $\boldsymbol{\delta}$ , from the equation

$$\sum_j h_{ij}\delta_j = -g_i, \quad (\text{C1})$$

where  $\mathbf{g}$  is the gradient of Gutzwiller Variational Energy with respect to Gutzwiller parameters. Provided that  $\mathbf{h}$  is positive-definite (and it can be modified to be so if necessary<sup>46</sup>), it can be convenient to solve Eq. (C1) within a smaller parameter space, defined by taking several Lanczos steps through the Hessian matrix  $\mathbf{h}$ . Also the memory storage of the algorithm can take great advantage of this possibility, since the definition of the Lanczos basis does not have as a requirement the knowledge of the full matrix  $h_{ij}$ , but only the knowledge of products  $h_{ij}x_j$ . Keeping in memory the full Hessian matrix is possible only for a small number of parameters, while it implies a considerable slow down of simulations in the case of

a 5-band Gutzwiller projector like the one we need for dealing with transition metals. Whenever we choose the starting Lanczos vector, we need to remember that finding an accurate solution for Eq. (C1) requires the solution vector  $\boldsymbol{\delta}$  to have a nonzero component on the first vector  $\mathbf{x}$  of the Lanczos chain. It can be shown that, provided  $\mathbf{h}$  is positive definite, the choice of the gradient  $\mathbf{g}$  as starting vector ensures that  $\boldsymbol{\delta}$  has nonzero components on the first three vectors of the Lanczos chain. Indeed, from the positive definiteness of  $\mathbf{h}$  descends that

$$\sum_{ij} \delta_i^* h_{ij} \delta_j > 0, \quad (\text{C2})$$

but since  $\boldsymbol{\delta}$  must be such that  $\sum_j h_{ij}\delta_j = -g_i$  (see Eq. (C1)), we have that

$$g_i^* \delta_i < 0, \quad (\text{C3})$$

so that  $\mathbf{g}$  has a nonzero component on  $\boldsymbol{\delta}$ . But we can say more than this, namely that there is a nonzero component of  $\boldsymbol{\delta}$  also on  $\mathbf{h}\mathbf{g}$ , since

$$\sum_{ij} \delta_j^* h_{ij} g_i = -\sum_{ij} (g_i^* h_{ij} \delta_j)^* = -\sum_j g_j g_j^* < 0 \quad (\text{C4})$$

provided that the gradient is finite. Finally, there is a nonzero component of  $\boldsymbol{\delta}$  also on  $\mathbf{h}^2\mathbf{g}$ , again due to the positive-definiteness of the Hessian, indeed

$$\begin{aligned} \sum_{ij} \delta_i^* [h^2]_{ij} g_j &= \sum_{ij} \left\{ g_i^* [h^2]_{ij} \delta_j \right\}^* = \\ &= -\sum_i \{g_i^* h_{ij} g_j\}^* < 0. \end{aligned} \quad (\text{C5})$$

This means that three Lanczos steps will certainly improve a steepest descent problem. Any further step will further refine the approximation to the correct descent direction  $\boldsymbol{\delta}$ . With the choice of the gradient as starting vector for the Lanczos chain, this minimization algorithm reduces to a constrained steepest descent in the limit of a single-vector Lanczos chain.

\* giovanni.borghi@epfl.ch, fabrizio@sissa.it, tosatti@sissa.it

<sup>1</sup> N. F. Mott, Proceedings of the Physical Society A **62**, 416 (1949).

<sup>2</sup> N. F. Mott, Metal Insulator Transition (Taylor and Francis, London, 1990).

<sup>3</sup> J. Hubbard, Proceedings of the Royal Society of London **276**, 238 (1963).

<sup>4</sup> W. M. C. Foulkes, L. Mitas, R. J. Needs, and G. Rajagopal, Rev. Mod. Phys. **73**, 33 (2001), URL <http://link.aps.org/doi/10.1103/RevModPhys.73.33>.

<sup>5</sup> U. Schollwöck, Rev. Mod. Phys. **77**, 259 (2005).

<sup>6</sup> A. Georges, G. Kotliar, W. Krauth, and M. J. Rozenberg, Rev. Mod. Phys. **68**, 13 (1996).

<sup>7</sup> V. I. Anisimov, J. Zaanen, and O. K. Andersen, Phys. Rev. B **44**, 943 (1991).

<sup>8</sup> F. A. V. I. Anisimov and A. I. Lichtenstein, Journal of Physics: Condensed Matter **9**, 767 (1997).

<sup>9</sup> V. I. Anisimov, D. E. Kondakov, A. V. Kozhevnikov, I. A. Nekrasov, Z. V. Pchelkina, J. W. Allen, S.-K. Mo, H.-D. Kim, P. Metcalf, S. Suga, et al., Phys. Rev. B **71**, 125119 (2005), URL <http://link.aps.org/doi/10.1103/PhysRevB.71.125119>.

<sup>10</sup> D. Ceperley, G. V. Chester, and M. H. Kalos, Phys. Rev. B **16**, 3081 (1977).

<sup>11</sup> S. Sorella, Physical Review B **71**, 241103 (2005).

<sup>12</sup> M. Marchi, S. Azadi, M. Casula, and S. Sorella, Journal of Chemical Physics **131**, 154116 (2009).

- <sup>13</sup> M. C. Gutzwiller, Phys. Rev. **134**, A923 (1964).
- <sup>14</sup> M. C. Gutzwiller, Phys. Rev. **137**, A1726 (1965).
- <sup>15</sup> J. Bünemann, W. Weber, and F. Gebhard, Phys. Rev. B **57**, 6896 (1998).
- <sup>16</sup> P. Fazekas, Lecture Notes on Electron Correlation and Magnetism (World Scientific Publishing, Singapore, 1999).
- <sup>17</sup> P. W. Anderson, Science **235**, 1196 (1987).
- <sup>18</sup> W. F. Brinkman and T. M. Rice, Phys. Rev. B **2**, 4302 (1970).
- <sup>19</sup> K. M. Ho, J. Schmalian, and C. Z. Wang, Phys. Rev. B **77**, 073101 (2008), URL <http://link.aps.org/doi/10.1103/PhysRevB.77.073101>.
- <sup>20</sup> X. Deng, L. Wang, X. Dai, and Z. Fang, Phys. Rev. B **79**, 075114 (2009).
- <sup>21</sup> T. Schickling, F. Gebhard, J. Bünemann, L. Boeri, O. K. Andersen, and W. Weber, Phys. Rev. Lett. **108**, 036406 (2012), URL <http://link.aps.org/doi/10.1103/PhysRevLett.108.036406>.
- <sup>22</sup> G. Wang, Y. Qian, G. Xu, X. Dai, and Z. Fang, Physical Review Letters **104**, 047002 (2010).
- <sup>23</sup> N. Lanatà, H. U. R. Strand, X. Dai, and B. Hellsing, Phys. Rev. B **85**, 035133 (2012), URL <http://link.aps.org/doi/10.1103/PhysRevB.85.035133>.
- <sup>24</sup> Y. X. Yao, C. Z. Wang, and K. M. Ho, International Journal of Quantum Chemistry **112**, 240 (2012), ISSN 1097-461X, URL <http://dx.doi.org/10.1002/qua.23238>.
- <sup>25</sup> N. Lanatà, Y.-X. Yao, C.-Z. W. Wang, K.-M. Ho, J. Schmalian, K. Haule, and G. Kotliar (2013), arXiv:1305.3950.
- <sup>26</sup> D. Vollhardt, N. Blümer, K. Held, and M. Kollar, in Band-Ferromagnetism, edited by K. Baberschke, M. Donath, and N. W. (Springer, Heidelberg, 2001), vol. 580 of Lecture Notes in Physics, pp. 191–207.
- <sup>27</sup> A. A. Katanin, A. I. Poteryaev, A. V. Efremov, A. O. Shorikov, S. L. Skornyakov, M. A. Korotin, and V. I. Anisimov, Phys. Rev. B **81**, 045117 (2010).
- <sup>28</sup> G. Stollhoff and P. Thalmeier, Zeitschrift für Physik B Condensed Matter **43**, 13 (1981), URL <http://dx.doi.org/10.1007/BF01295470>.
- <sup>29</sup> J. B. Goodenough, Phys. Rev. **120**, 67 (1960).
- <sup>30</sup> M. B. Stearns, Physical Review B **8**, 4383 (1973).
- <sup>31</sup> J. M. D. Coey, M. Viret, and S. von Molnár, Advances in Physics **48**, 167 (1999), <http://www.tandfonline.com/doi/pdf/10.1080/000187399243455>, URL <http://www.tandfonline.com/doi/abs/10.1080/000187399243455>.
- <sup>32</sup> M. Levy, Proc. Natl. Acad. Sci. USA **76**, 6062 (1979).
- <sup>33</sup> M. Levy, Phys. Rev. A **26**, 1200 (1982).
- <sup>34</sup> E. Lieb, Int. J. Quantum Chem. **24**, 243–77 (1983).
- <sup>35</sup> P. Hohenberg and W. Kohn, Phys. Rev. **136**, B864 (1964).
- <sup>36</sup> T. Körzdörfer, Journal of Chemical Physics **134**, 094111 (2011).
- <sup>37</sup> A. G. Petukhov, I. I. Mazin, L. Chioncel, and A. I. Lichtenstein, Phys. Rev. B **67**, 153106 (2003).
- <sup>38</sup> M. Cococcioni and S. de Gironcoli, Phys. Rev. B **71**, 035105 (2005).
- <sup>39</sup> A. I. Liechtenstein, V. I. Anisimov, and J. Zaanen, Phys. Rev. B **52**, R5467 (1995), URL <http://link.aps.org/doi/10.1103/PhysRevB.52.R5467>.
- <sup>40</sup> K. Haule and G. Kotliar, New Journal of Physics **11**, 025021 (2009).
- <sup>41</sup> Z. P. Yin, K. Haule, and G. Kotliar, Nature Materials Research Bulletin **10**, 932 (2011), URL <http://www.nature.com/nmat/journal/v10/n12/full/nmat3120.html>.
- <sup>42</sup> Z. P. Yin, K. Haule, and G. Kotliar, Nature Physics **7**, 294 (2011), URL <http://www.nature.com/nphys/journal/v7/n4/full/nphys1923.html>.
- <sup>43</sup> S. Sorella, Phys. Rev. B **64**, 024512 (2001), URL <http://link.aps.org/doi/10.1103/PhysRevB.64.024512>.
- <sup>44</sup> F. Aryasetiawan, M. Imada, A. Georges, G. Kotliar, S. Biermann, and A. I. Lichtenstein, Phys. Rev. B **70**, 195104 (2004), URL <http://link.aps.org/doi/10.1103/PhysRevB.70.195104>.
- <sup>45</sup> N. Lanatà, P. Barone, and M. Fabrizio, Phys. Rev. B **78**, 155127 (2008).
- <sup>46</sup> R. Fletcher, Practical Methods of Optimization (John Wiley & Sons, 1987).
- <sup>47</sup> C. Corliss and J. Sugar, J. Phys. Chem. Ref. Data **11** (1982).
- <sup>48</sup> R. D. Cowan, Theory of Atomic Structure and Spectra (University of California Press, 1981).
- <sup>49</sup> W. Setyawan and S. Curtarolo, Computational Materials Science **49**, 299 (2010), ISSN 0927-0256, URL <http://www.sciencedirect.com/science/article/pii/S0927025610002697>.
- <sup>50</sup> C. Zener, Physical Review **82**, 403 (1951).
- <sup>51</sup> P. W. Anderson and H. Hasegawa, Phys. Rev. **100**, 675 (1955), URL <http://link.aps.org/doi/10.1103/PhysRev.100.675>.
- <sup>52</sup> E. C. Stoner, Proceedings of the Royal Society A **165**, 372 (1938).
- <sup>53</sup> J. Sánchez-Barriga, J. Braun, J. Minár, I. Di Marco, A. Varykhalov, O. Rader, V. Boni, V. Bellini, F. Manghi, H. Ebert, et al., Phys. Rev. B **85**, 205109 (2012), URL <http://link.aps.org/doi/10.1103/PhysRevB.85.205109>.
- <sup>54</sup> J. Sánchez-Barriga, J. Braun, J. Minár, I. Di Marco, A. Varykhalov, O. Rader, V. Boni, V. Bellini, F. Manghi, H. Ebert, et al., Phys. Rev. B **85**, 205109 (2012), URL <http://link.aps.org/doi/10.1103/PhysRevB.85.205109>.
- <sup>55</sup> M. Karolak, G. Ulm, T. Wehling, V. Mazurenko, A. Poteryaev, and A. Lichtenstein, Journal of Electron Spectroscopy and Related Phenomena **181**, 11 (2010), ISSN 0368-2048, <http://www.sciencedirect.com/science/article/pii/S0368204810001222>.
- <sup>56</sup> W. Weber, J. Bünemann, and F. Gebhard, arXiv:010.7033v1 (2001).
- <sup>57</sup> J. Bünemann, F. Gebhard, T. Ohm, S. Weiser, and W. Weber, in Frontiers in Magnetic Materials, edited by A. Narlikar (Springer, Berlin, 2005), pp. 117–151.
- <sup>58</sup> J. Bünemann, F. Gebhard, T. Ohm, S. Weiser, and W. Weber, Phys. Rev. Lett. **101**, 236404 (2008).
- <sup>59</sup> T. Inui, Y. Tanabe, and Y. Onodera, Group Theory and Its Applications in Physics (Springer, New York, 1996).
- <sup>60</sup> M. Tinkham, Group Theory and Quantum Mechanics (Dover, 1964).
- <sup>61</sup> Z. Gimbutas and L. Greengard, Journal of Computational Physics **228**, 5621 (2009), URL <http://www.sciencedirect.com/science/article/pii/S0021999109002691>.
- <sup>62</sup> Note1, the quantum number  $L$  is still used to label states since each irreducible representation of the cubic group comes from a definite representation of the rotation group

$O(3)$ . However, in the case of cubic symmetry  $L$  is no longer a conserved quantum number, and the ground-state of the

Hamiltonian will not necessarily have a definite  $L$ .